Granitoid zircon forms the nucleus for minerals precipitated by carbonatite-derived metasomatic fluids at Chilwa Island, Malawi

Emma Dowman[a,b,c], Frances Wall[b,c], Teresa Jeffries[c*], Peter Treloar[a], Andrew Carter[d] , Andrew Rankin[a]
[a]School of Geography, Geology & Environment, Kingston University, Penrhyn Road, Kingston upon Thames, KT1 2EE, UK
[b]Camborne School of Mines, University of Exeter, Cornwall Campus, Penryn, Cornwall, TR10 9FE, UK
[c]Department of Mineralogy, Natural History Museum, Cromwell Road, London, SW7 5BD, UK
[d]Department of Earth and Planetary Sciences, Birkbeck College, Gower Street, London, WC1E 7HX, UK

Abstract

Mineralogical assemblages are fundamental to the interpretation of geological processes. Zircon is an integral petrographic component of the mineral assemblages present in fenites (rocks formed by alkaline metasomatism) associated with the 136 Ma-aged Chilwa Island carbonatite complex, Malawi. Zircon exhibits contrasting characteristics and properties across the fenite aureole that surrounds the carbonatite stock. It shows intense grain dissolution and subsequent replacement by pyrochlore in the more intensely metasomatised 'high-grade' fenite of the innermost part of the aureole. By contrast, relict zircon crystals form the nucleus for the development of apatite-ilmenite-REE mineral assemblages in less altered zones. These changes in zircon properties are considered to be evidence of the diverse nature of fluids that metasomatised the Chilwa Islands fenite aureole. Although zircon is a principal component of the fenite mineral assemblages, when dated by LA-ICP-MS techniques it was found to predate the other minerals present in the mineral assemblages and thus, the age of carbonatite intrusion, by over 380 Ma. Instead of co-crystallising with the assemblage, zircon is therefore interpreted as providing a focus around which the minerals in the fenite assemblage formed. This implies that caution is needed both in the interpretation of Zr mobility in metasomatic assemblages, and also in attributing a zircon age to the assemblage as a whole in such sequences.

Keywords: zircon; geochronology; fenite; metasomatism; carbonatite

1. Introduction

Zircon is the most commonly used, and therefore perhaps the most important, mineral in geochronology. Among the properties that make it useful for dating are its chemical durability and stability (Harley and Kelly, 2007; Siebel et al., 2012 and citations therein) and its low solubility in most geological fluids. However, it has been shown that zircon can be soluble in certain alkaline fluids (Rubin et al., 1993; Sheard et al., 2012). It is therefore possible that zircon breakdown and subsequent Zr mobility and reprecipitation might be expected in fenites developed by alkali metasomatism around carbonatite intrusions. These metasomatised rocks are created by the early expulsion of alkaline fluids associated with carbonatite or ijolite emplacement (Heinrich, 1966; Le Bas, 2008).

A better understanding of fenite aureoles is important first, to the overall hypothesis of petrogenesis of carbonatites and alkaline rocks because fenite holds important information on the amounts of alkalis and volatile elements in the original magmas and, second, because carbonatites and alkaline rocks are associated with many of the world's principal concentrations of rare earth elements (REE) and high field strength elements (HFSE) such as niobium, as well as apatite and fluorite deposits (Mariano, 1989;

Berger et al., 2009; Goodenough et al., 2017; Verplanck et al., 2016; Mitchell, 2015 and citations therein). Ore-forming processes range from magmatic fractionation to hydrothermal reworking and even late-stage fluids are now known also to pervade fenite aureoles (Verplanck and Van Gosen, 2011; Dowman et al., 2017).

This study has two, closely interlinked aims. The main aim is to understand better the behaviour of zircon during fenitisation and the potential mobility of Zr in fenitising solutions. The secondary aim was to date the zircon and apatite to constrain better the ages of Pan-African events in East Africa as well as the age of carbonatite emplacement. The metasomatic aureole around the Chilwa Island Carbonatite Complex in southern Malawi was chosen for this study. This is because although zircon is rare in carbonatites due to low silica activity (Barker, 2001), it is a common accessory phase in micro-assemblages of metasomatic minerals in the fenite at Chilwa Island. Petrographically, it appears to have been an integral component during precipitation of fenite minerals and should provide a good way to date the fenite, and thereby also the intrusion of the carbonatite. However, contrary to the petrographic evidence, new U-Pb isotopic age dating reported here shows that the zircon crystals in the micro-mineral assemblages are much older than the fenite. This paper describes and discusses this finding, including its implications for use of zircon in geochronology studies of alkaline systems and the implications for understanding the mobility of HFSE in and around alkaline rocks and carbonatites.

2. Geological setting

The focus of this study is the Chilwa Island Cretaceous apatite-magnetite-rich carbonatite ring complex of the Chilwa Alkaline Province (CAP) of Malawi at the extreme southern end of the East African Rift system.

In the CAP, the host basement rocks are amphibolite and granulite facies gneisses, schists and amphibolites of the East African Orogen. They record a complex, and not fully understood, history comprising the aggregation and dispersal of Rodinia (~1300 to ~800 Ma) and subsequent formation of Gondwana (~800 to ~550 Ma) (Kröner et al., 2001), which was accompanied by the extensive emplacement of predominantly calc-alkaline granitoids between ~840 and <600 Ma (Kröner, 2001). Tectonically part of the Mozambique Belt, the rocks underwent high-grade metamorphism in the period 571-549 Ma (Kröner and Stern, 2005). Terrestrial sedimentation and volcanism of the Karoo Supergroup in Permian to Jurassic times was followed by alkaline magmatism in the CAP, driven by crustal extension and decompressional melting, between 138 and 107 Ma (Eby et al., 1995). This produced seventeen carbonatite intrusions, in two main belts: a western belt associated with lines of rifting, and an eastern chain within a zone of depression (Garson, 1965).

Chilwa Island is located at the northern end of the eastern chain of carbonatite centres, in the southwest of Lake Chilwa. The largest of the Malawi carbonatites, it is a ring complex ca. 4 km in diameter, consisting of multiple carbonatite intrusions (Fig 1). Structural relationships indicate sequential emplacement from early outer calciocarbonatites (commonly termed ‘sövite’) inwards to later ankeritic (increasing Mg, Fe) carbonatites and then to the youngest central sideritic (Fe-, Mn-rich) carbonatite (Garson and Campbell Smith, 1958; Garson, 1965; Le Bas, 1981; Woolley, 2001).

Brecciated country rock and fenitised Precambrian granulites surround the carbonatite rocks (Fig 1). The outer margins of alteration of the country rock are hidden beneath the lake and its sediments. No completely unaltered rock is found in the island. A time frame for the complex is provided by K-Ar dating of biotite in the earliest (calcio)carbonatite by Snelling (1965) at 138 Ma, and by Eby et al. (1995), who used titanite fission-track analysis to date a nepheline-syenite plug intruding carbonatite at 126 Ma, with apatite fission-track dates of 87±9 Ma from the same rock.

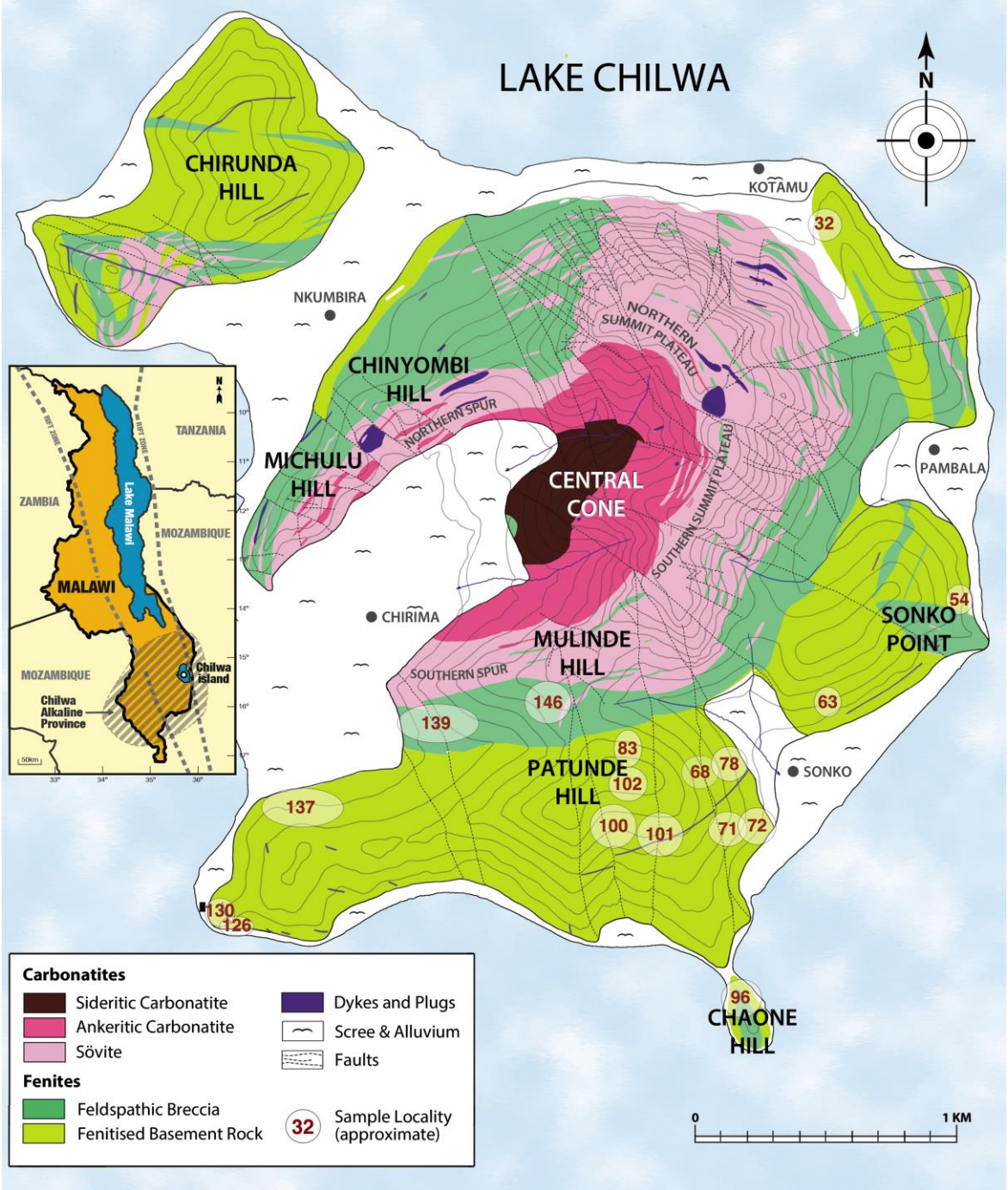

Fig 1 Geological map of Chilwa Island carbonatite complex (adapted from Garson, 1958) with approximate location of samples used in study

Garson and Campbell Smith (1958) proposed metasomatism of the aureole by several pulses of fenitisation, with alkaline fluids channelled along a network of veins and grain boundaries in the rocks. They undertook a comprehensive survey of the mineralogy of the fenite rocks, which they divided into three groups with reference to the effects of the intensity of metasomatism. The outermost carbonatite is surrounded by a collar of potassic feldspathic breccia. The breccia is end-stage or high-grade fenite, probably broken up during episodes of high pressure during the history of the carbonatite central complex. Outside the breccia lies fenitised country rock, divided by Woolley (1969) into a less fenitised group of 'quartz fenites' and an inner group of 'syenitic fenites'. The mineralogy of the less altered quartz fenites is inherited primarily from the basement and is dominated by plagioclase and quartz, with minor aegirine also present. In the syenitic fenites, quartz and plagioclase have been replaced by a new mineralogy of orthoclase, aegirine and sodic amphiboles such as magnesio-arfvedsonite, and minor albite. A transition from sodic-dominated to potassic fluids is thought to have occurred during the course of fenitisation (Woolley, 1969; Dowman, 2014).

3. Methodology

A selection of rocks from across the fenite aureole was chosen for investigation from the collection held by the Natural History Museum, London (BM 1968 P37). These included two breccia samples, four samples from medium/high grade fenite, seven medium-grade fenite examples and three from low-grade fenite (Fig 1 for locations, see Supplementary Table 1 for individual sample details).

An analytical SEM was used for phase identification, and to determine the pattern, distribution and mineral associations of zircon in each grade of fenite. This was carried out at Kingston University on a Zeiss EVO 50 scanning electron microscope (SEM) fitted with a BSE detector, Oxford Instruments analytical suite (INCA) comprising an INCA X-act energy dispersive spectrometer (EDS), an INCA Wave wavelength dispersive spectrometer (WDS) and a Gatan Chroma-CL cathodoluminescence detector. For EDS, the operating conditions of the microscope used an accelerating voltage of 20kV with a beam current of 1-1.8 nA. Spot size is defined by the beam current and is approximately 5µm. Cathodoluminescent imaging of zircon and apatite used an accelerating voltage of 10-15 kV and a beam current of 1-5 nA.

Analysis of zircon trace element mineral chemistry was undertaken to determine whether grains from different parts of the aureole comprise a single population. Zircons in medium- and low-grade fenite were also dated to establish whether they could have had a carbonatitic inheritance. Dating and analyses of zircon from separates and in thick section were obtained via Laser Ablation Inductively Coupled Plasma Mass Spectrometry (LA-ICP-MS) using the instrument at the Natural History Museum, London. This comprised a New Wave UP193FX Laser Ablation System coupled to Agilent 7500cs ICP-MS. Trace elements were determined using NIST 612 as an external reference standard and SiO_2 as an internal standard. Si values for internal standardisation were determined by SEM/EDS. The natural zircon standard 91500 was used in U-Pb age determinations. In both cases, sample transport was achieved using a He gas flow. For trace element analyses data were collected for 90s, using spot sizes between 20-30µm, and

laser fluence of 3.2 J/cm^2 firing at 10Hz. Isotopic data (^{207}Pb/^{235}U and ^{206}Pb/^{238}U) were collected using line rasters of approximately 50-70 μm long with a beam diameter of 25-30 μm. Data were collected for 135s using a laser fluence of 2.6 J/cm^2 firing at 10Hz.

Zircon is considered to be generally virtually free of initial common Pb (^{204}Pb) (Corfu, 2013), possibly because its assumed divalent state is not particularly compatible with zircon structure (Chew et al., 2017). As part of the control process, Hg counts were checked for background levels and if these had risen when the samples were analysed, then the zircon would have been rejected. A further control was to analyse multiple grains from the same sample, as it is unlikely that all grains would contain the same amount of common Pb (Kröner et al., 2014).

Apatite fission track analysis was also applied to a low-grade fenite sample to provide additional information regarding mineral assemblages and metasomatising fluids. The sample preparation, and FT analysis was made at the UCL-Birkbeck London Geochronology Centre. Separated apatite grains were mounted and polished for etching. Etching used 5N HNO_3 at 20˚ ± 1˚C for 20 seconds. Etched grain mounts were packed with mica external detectors and Corning glass (CN5) dosimeters and irradiated in the FRM 11 thermal neutron facility at the University of Munich, Germany. Following irradiation the external detectors were etched using 48% HF at 20˚C for 25 minutes. Sample ages were determined using the zeta calibration method and IUGS recommended age standards (Hurford, 1990).

The study of fluid inclusions to characterise the metasomatising fluids included microthermometry. This was carried out at Kingston University using a TMS600 mechanical heating and cooling stage with Tm94 Controller and Linksys 32 software, and attached to a Nikon Optiphot with x5, x10 and x40 LWD lenses. CO_2 and H_2O standards were used for calibration.

Raman spectroscopic analysis of double-polished sections was carried out at Kingston University using a Renishaw RM1000 instrument with CCD detection via WIRE 1.3 software. A silicon standard with a single peak at 521 cm^{-1} was used, and runs were for 20s using a 514 nm Ar ion laser. Qualitative SEM-EDS analysis of the contents of inclusions exposed on the freshly broken surfaces of quartz samples was also carried out after coating fragment edges in Au and Pd.

4. Results

4.1 Distribution and morphology of zircon in the metasomatised aureole

Our mineralogical study identified four stages of fenitisation in the aureole around the carbonatite at Chilwa Island. These are graded according to the degree of alteration of the country rock gneisses by alkaline metasomatic fluids, and are described below. The terminology of low-grade and medium-grade fenite is used instead of ‘quartz fenite’ and ‘syenite fenite’ respectively. It was noted that zircon habit varies considerably with the intensity of fenitisation.

Low-grade fenite has a matrix of quartz and plagioclase, and is found about 1 km from the carbonatite. Mineralised veins are scarce and usually comprise aegirine and

K-feldspar, with only a few assemblages containing apatite, rutile and ilmenite. Zircons occur infrequently in these rocks, tend to form lozenge-shaped grains, 40 to 80 μm in size and subeuhedral in form with zoning rarely visible under backscattered electron imaging (Fig 2a). Under visible light CL imaging, these zircons show blue shades but with dark cores and lighter overgrowths. CL imaging shows that the zircons are generally located in association with K-rich feldspar in veins of (fenite-related) alteration (Fig 2b).

Zircon occurs more frequently in the medium-grade fenite group. Rocks of this zone contain less quartz, but host more K-feldspar and extensive aegirine mineralisation, concentrated in veins. Zircon is 30 to 150 μm in size, and is euhedral to subeuhedral in shape, similar to grains in the lower-grade fenite. It displays a striking distribution pattern, being almost exclusively present in mineral assemblages associated with these veins. The assemblages are the main characteristic of this grade of fenite, consisting of zircon together with fluorapatite with inclusions of monazite ($CePO_4$) of a few microns in size, ilmenite, rutile (both Nb-bearing), magnetite and occasional bastnäsite ($Ce(CO_3)F$ (Fig 2c). In thin section, apatite is also seen to be present in embayments and as 'inclusions' in zircon. CL imaging of the mineral assemblages shows that the apatites contain multiple zones, and that the altered feldspar, which typically surrounds these assemblages, luminesces bright scarlet (Fig 2d). The zircons themselves are blue, with fine oscillatory zoning, often with dark cores and brighter overgrowths and their intricate association with the purple-luminescing apatite is apparent (Fig 2f). The blue colour displayed by zircon probably results from Dy^{3+} activation and/or from electron defects on the SiO_4 groups (Götze et al., 1999). Radioactive decay of trace U is thought to be one of the causes of yellow luminescence of zircon (Hanchar et al., 2001), which is evidence that the blue zircons at Chilwa Island are non-metamict in nature.

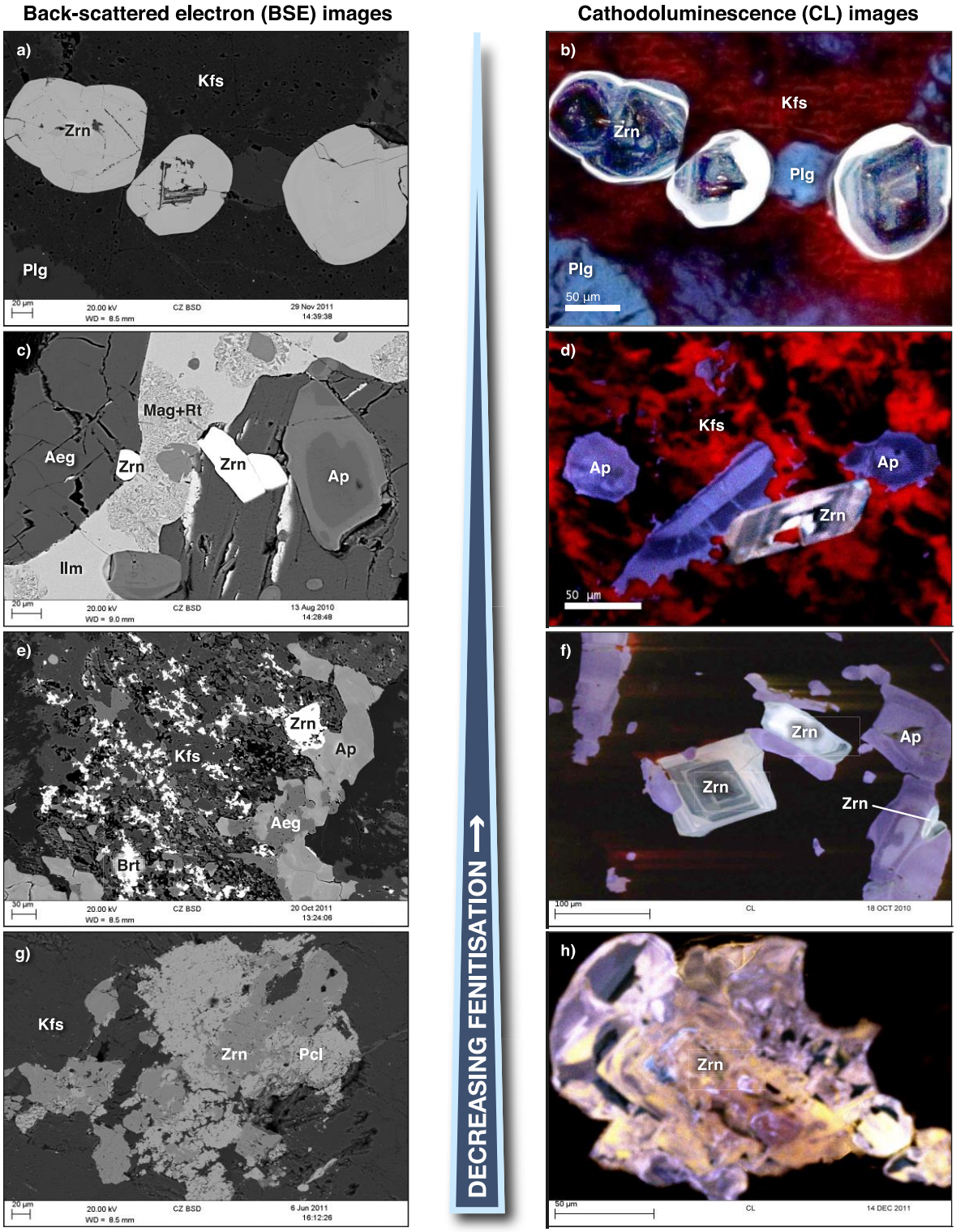

Fig 2 Images illustrating style of zircon in fenite zones at Chilwa Island
a) BSE image of zircons in low-grade fenite BM1968 P37 72
b) CL image of zircons in low-grade fenite BM1968 P37 72, zoning clearly visible
c) BSE image of typical zircon-apatite-ilmenite assemblage in medium-grade fenite BM1968 P37 78 with areas of magnetite-rutile separation within ilmenite grains
d) CL image of typical zircon-apatite-ilmenite assemblage in medium-grade fenite BM1968 P37 32 (note: ilmenite is CL quencher and scarlet is fenite altered feldspar)
e) BSE image of zircon in higher grade fenite BM1968 P37 54: remnant of mineral assemblage, starting to

resorb/dissolve

f) CL image of detail of zircon/apatite association in medium-grade fenite BM1968 P37 96

g) BSE image of zircon, pyrochlore assemblage in K-feldspar (orthoclase) breccia BM1968 P37 146

h) CL image of porous zircon in K-feldspar (orthoclase) breccia BM1968 P37, interpreted as a dissolution texture.

A more altered subgroup is found within the medium-grade fenites. This is dominated by a mineralogy of aegirine and K-feldspar (orthoclase), accompanied by minor albite, fluorapatite without zoning, rutile and recrystallised quartz. Minerals such as barite ($BaSO_4$), the rare-earth fluorcarbonate, parisite ($CaCe_2(CO_3)F_2$), and carbonates (calcite and ankerite) are present. However, only vestiges of the zircon-apatite-ilmenite mineral assemblages characteristic of the main medium-grade group remain. Zircon is now scarce. Examples of the usual lozenge-shaped grains, with clean outlines, persist in the assemblage remnants. However, where zircon occurs in aegirine, it appears ragged in shape and of a filigree texture, as though undergoing resorption (Fig 2e and Fig 3a-c). Rare occurrences of zircon grains, only a few microns in size, are seen in porous fluorapatite and rutile.

The highest grade of 'fenitised' rocks at Chilwa Island is seen in the breccias. These are of an almost monophase K-feldspar composition, and form a "collar" around the carbonatite. Aegirine is absent, as are the zircon-apatite-ilmenite assemblages of the medium-grade fenites. Recrystallised quartz occurs occasionally. Carbonatite-associated minerals include a scarce Th-RE phosphate phase, goyazite ($SrAl_3(PO_4)_2(OH)_5 \bullet \{H_2O$) and bariopyrochlore ($(Ba,Sr)(Nb,Ti)_2(O,OH)_7$, this last being a mineral known to associate with carbonatite (Hogarth, 1989), and now termed a kenopyrochlore by the International Mineralogical Association (IMA). Zircon is uncommon in this zone. It occurs as groups of ragged and porous grains, and is associated with pyrochlore, which appears to have replaced the zircon (Figs 2g and 3d). Under CL imaging, zircons are mostly yellow in colour, with patches of blue/purple (Fig 2h). The yellow colour may result from lattice defects arising from activation of impurities (Tsuchiya et al., 2015, and references therein) during metasomatism rather than from radiation damage. No evidence of reprecipitation of Zr into Zr-bearing alkali-rich minerals was found.

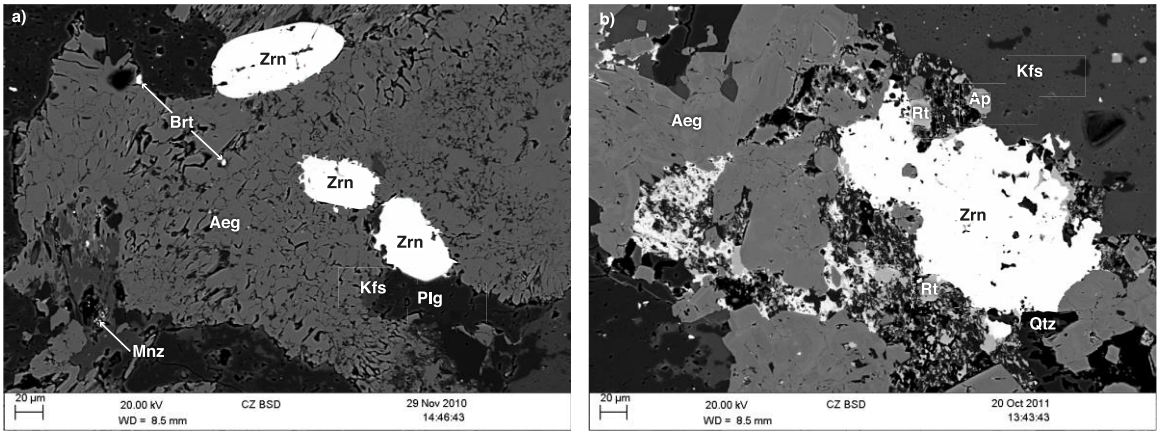

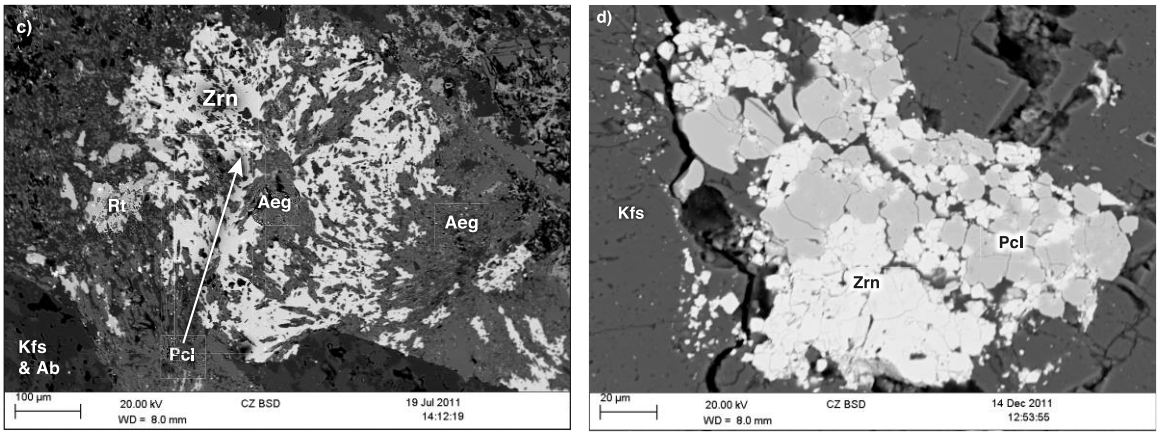

Fig 3 Backscattered electron images illustrating instability of zircon during reaction with metasomatising fluids
a) low-grade fenite BM1968 P37 71 zircon grains showing first indication of dissolution along aegirine contact
b) and **c)** medium/high-grade fenite BM1968 P37 54 and 102 zircon grains undergoing progressive dissolution with increasing fenitisation
d) breccia BM1968 P37 146 zircon/pyrochlore association characteristic of breccia

4.2 Geochronology – zircon

U-Pb isotope data from Chilwa Island zircons are set out in Supplementary Table 2. CL imaging indicated the existence of core-mantle-rim structures in some zircon grains, particularly those from low-grade fenite, but the spatial resolution of the technique (>5 μm) was insufficient to analyse these zones separately. Data from low-grade zircon is also more discordant than zircon data from medium-grade fenite, but the cause of the discordancy could not be determined. One possibility is the loss of different amounts of Pb from grains during fluid interaction due to variation in grain size and crystal defects. This is thought to permit the parallel existence of concordant and discordant domains (Corfu, 2013). An alternative explanation is that discordancy results from the presence of mixed domains within grains, for example, those comprising an older core and a younger rim. However, mixing produces severely discordant data (Corfu, 2013) and might only explain the most discordant results obtained for Chilwa Island zircons. It is thus possible that both these factors operated, and that zircon was experiencing conditions in an open system, with events when isotopic reset could have occurred.

The U-Pb concordia ages obtained from zircon are all considerably older than the 136 Ma age published for the Chilwa Island carbonatite (Eby et al., 1995), and also much older than any of the other rocks in the Chilwa Alkaline Province. Fig 4 plots concordant results. Zircon separates from medium-grade fenite produced a date of 520±2.3 Ma and a similar date of 516±2.9 Ma was generated from in situ dating of zircon within a polished thick section (Fig 4a-b).

Zircon grains from low-grade fenite produced a number of concordant points, four of which clustered at 769±5 Ma (Fig 4c). A plot of all concordant grains (blue ellipses) from the low-grade fenite sample traces a line of discordia (Fig 4d), where intercepts with the concordia curve are believed to represent the formation age of the zircon grains (the upper intercept) and a later event that caused isotopic resetting of grains (the lower intercept). The lower intercept falls at c.520 Ma, which is the concordia age of the medium-grade zircons. Fig 4e plots concordant grains from all three samples, with intercepts on the line of discordia at c.812 Ma and c.511 Ma.

The zircon dates obtained could be interpreted as representing the age of the basement and of a younger intrusive or metamorphic event. The evidence for this is considered in the discussion.

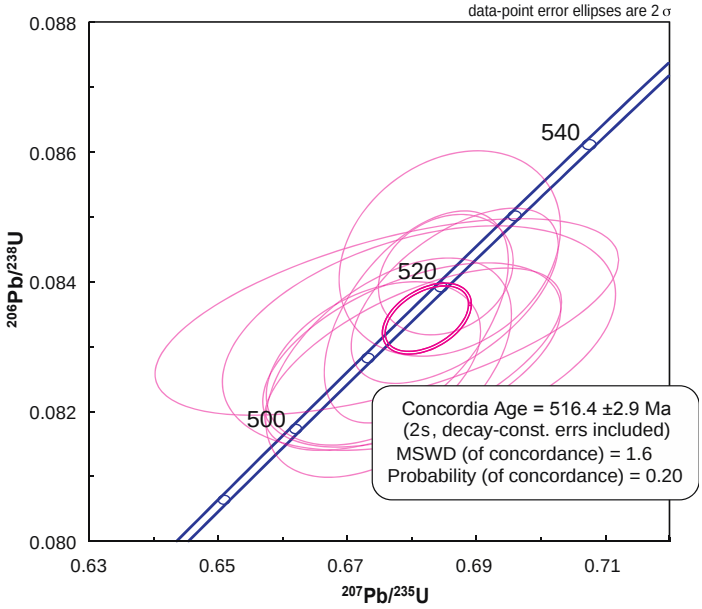
data-point error ellipses are 2 σ
0.088
0.086
0.084
0.082
0.080
0.63
0.65
0.67
0.69
0.71
206Pb/238U
207Pb/235U
540
520
500
Concordia Age = 516.4 ±2.9 Ma
(2s, decay-const. errs included)
MSWD (of concordance) = 1.6
Probability (of concordance) = 0.20

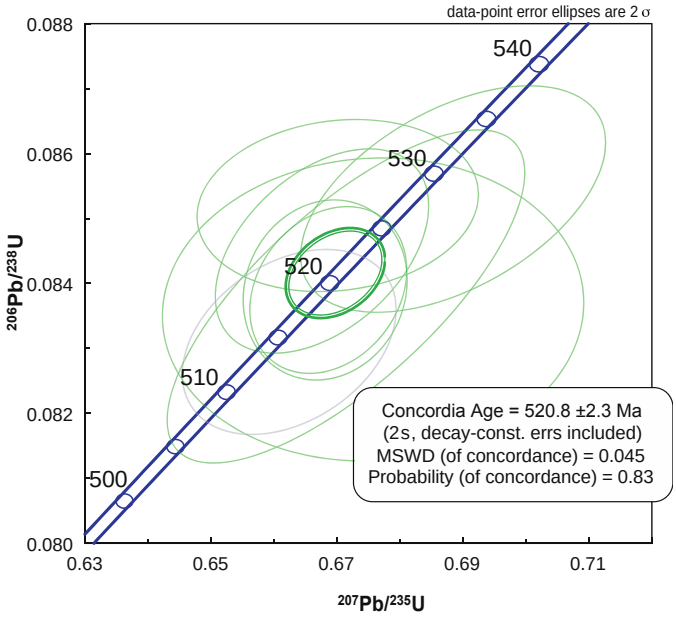
data-point error ellipses are 2 σ
0.088
0.086
0.084
0.082
0.080
0.63
0.65
0.67
0.69
0.71
206Pb/238U
207Pb/235U
540
530
520
510
500
Concordia Age = 520.8 ±2.3 Ma
(2s, decay-const. errs included)
MSWD (of concordance) = 0.045
Probability (of concordance) = 0.83

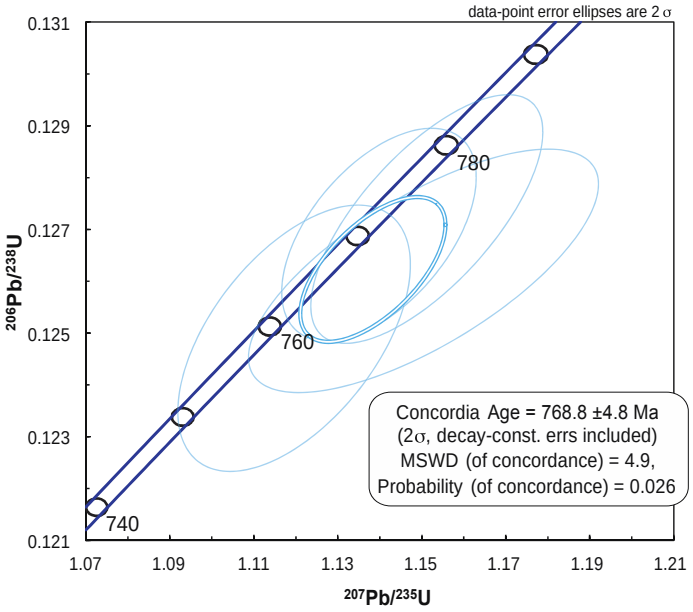
data-point error ellipses are 2 σ
0.131
0.129
0.127
0.125
0.123
0.121
206Pb/238U
1.07
1.09
1.11
1.13
1.15
1.17
1.19
1.21
207Pb/235U
740
760
780
Concordia Age = 768.8 ±4.8 Ma
(2σ, decay-const. errs included)
MSWD (of concordance) = 4.9,
Probability (of concordance) = 0.026

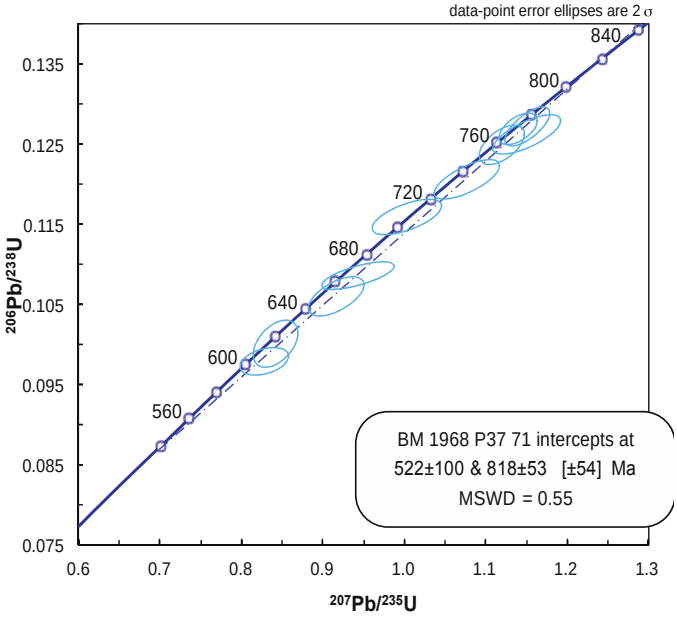
data-point error ellipses are 2 σ
0.135
0.125
0.115
0.105
0.095
0.085
0.075
206Pb/238U
0.6
0.7
0.8
0.9
1.0
1.1
1.2
1.3
207Pb/235U
560
600
640
680
720
760
800
840
BM 1968 P37 71 intercepts at
522±100 & 818±53 [±54] Ma
MSWD = 0.55

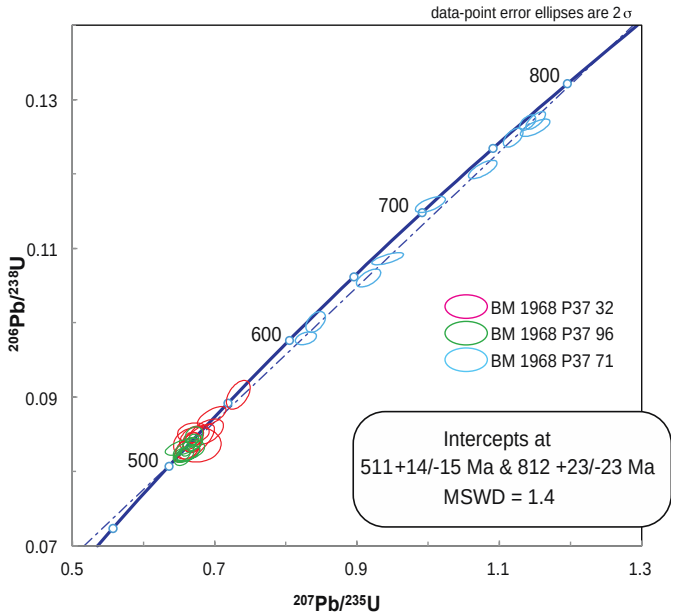

Fig 4 U-Pb concordia diagrams for zircon from Chilwa Island
a) separates from medium-grade fenite BM1968 P37 32
b) in-situ in thick section from medium-grade fenite BM1968 P37 96
c) group of four grains from separates from low-grade fenite BM1968 P37 71
d) all concordant grains for low-grade fenite BM1968 P37 71 showing line of discordia
e) all concordant grains for samples BM1968 P37 32, BM1968 P37 96 and BM1968 P37 71 showing line of discordia

Determinations are by LA-ICP-MS. All ellipses are plotted at 2s level of uncertainty.
The concordia age solution in Fig 4a-c for each sample is shown as a thicker ellipse. Other ellipses relate to individual grains.

4.3 Thermochronometry – apatite

Apatite fission track analysis was made of grains separated from an example of a low-grade fenite containing a few examples of micro-mineral assemblages of zircon, apatite and ilmenite (BM1968 P37 71). A fission track central age of 99±4 Ma was obtained (Fig 5a, Supplementary Table 3). A thermal history model of the age and track length distribution used to constrain cooling history indicates that apatite cooled to c. 60˚C at around 120 Ma and has since remained below that temperature, thus being at or near the surface (Fig 5b). These results are therefore compatible with the dates previously reported for carbonatite/alkaline rocks by Snelling (1965) and Eby et al. (1995) (Fig 5c), and also with the tectonic history of the area since carbonatite emplacement, which is of uplift with no suggestion of any post-emplacement burial.

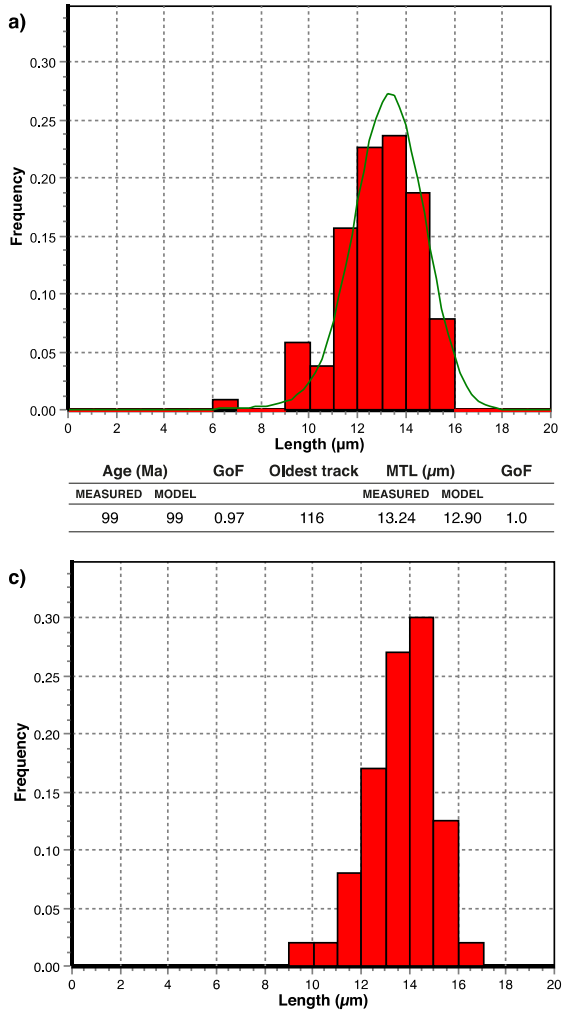

Fig 5 Results of apatite fission track dating using the program HeFty (Ketcham, 2005) with DPAR data to constrain annealing based on Ketcham et al. (2007)

a) Histogram of track length distribution from Chilwa Island low-grade fenite BM1968 P37 71

b) Model of time/temperature history in this apatite, showing cooling below 60˚C at c.120 Ma during the episode of carbonatite emplacement

c) Apatite track length distribution from Chilwa Island nepheline syenite for comparison with (a) (adapted from Eby et al., 1995)

An important question is determining whether the apatite relates to the evolution of the basement (and is contemporary with zircon), was reset during fenitisation and is contemporary with carbonatite emplacement or simply records the unroofing history. Apatite fission track thermochronometry records the last time that the mineral cooled through the fission track partial annealing zone from temperatures of c.120˚C to 60˚C. Any apatite that might have formed part of the original basement complex would probably have been buried at a depth of around two kilometres at the time of carbonatite emplacement (Garson and Campbell Smith, 1958) and is likely to have largely cooled beyond the partial annealing zone, assuming a thermal gradient of 25˚C km^{-1}. Fission tracks in any such original apatite at this stage would relate to the time of this cooling. A subsequent influx of metasomatic fluids could have wholly or partially erased these fission tracks, depending on peak fluid temperature in different parts of the aureole, and new fission tracks would form on post-metasomatic cooling.

Although the distribution of the minerals in the assemblages indicates that the apatite postdates zircon, in the absence of an absolute age for apatite, the possibility that both minerals first formed in basement rocks cannot be entirely discounted. However, a metasomatic origin rather than a basement origin for apatite is supported by the following evidence.

Much of the carbonatite at Chilwa Island is apatite-rich, but contains no zircon. The magmatic/metasomatic environment was thus favourable for apatite formation.

Apatite in medium-grade fenite contains REE (Supplementary Table 4), and zonation in grains reflects a varying REE content. The basement rock is not considered to be REE-enriched and apatite is not among its main primary minerals.

Cathodoluminescence colours are believed to arise from chemical impurities (activators) within the crystal structure of a mineral and/or from lattice defects (Götze et al., 1999). In common with apatite mineralisation related to alkaline rocks and carbonatites, Chilwa Island fenite apatite exhibits lilac/violet colours under cathodoluminescence (Dowman, 2014) which are attributed to the activity of the REE ions Ce^{3+}, Eu^{2+}, Sm^{3+}, Dy^{3+} and Nd^{3+}, and also Eu^{3+}, although this is not a reflection of the relative element concentrations (Waychunas, 2002; Kempe and Götze, 2002; Rae et al., and references therein, 1996; Hayward and Jones, 1991). The activation of Mn^{2+}, an ion relatively depleted in many carbonatites, is believed to produce the yellow to orange CL colour typically observed in apatite from granitic rocks (Kempe and Götze, 2002; Mariano, 1988). Coulson and Chambers (1996) noted yellow to buff luminescence in apatite in unmetasomatised rocks contrasting with blue/purple colours in apatite in fenitised rocks. If the Chilwa Island fenite apatite is of basement age, we might therefore expect to observe yellow grains with purple overgrowths relating to the later metasomatic event, but no example of this pattern was seen. CL colours support a carbonatite-related origin for the apatite.

Apatite persists in medium/high-grade fenite where zircon is being resorbed. If both minerals are originally from the basement rocks, then zircon might be expected to be the more robust. The appearance of the minerals suggests that the metasomatic fluids promoted apatite formation and zircon dissolution.

The apatite grains used for fission track analysis come from a low-grade fenite, where metasomatic fluids would have been lower in temperature. If the apatite pre-dated fenitisation and contained pre-carbonatite fission tracks, it may be that the fluids would not have been sufficiently hot to reset all of these earlier tracks, in which case analysis might reveal a more complex track length distribution and show overdispersion of grains ages. Only one population is seen in the results in Fig 5.

4.4 Zircon geochemistry

Zircons from low-grade fenite (BM1968 P37 71) and from medium-grade fenites (BM1968 P37 32 and BM1968 P37 96) were analysed for REE, Hf and Pb content using laser ablation techniques (Supplementary Table 5). Zircon major element composition was obtained by analytical SEM (Supplementary Table 6).

A chondrite-normalised REE graph and a normal distribution plot for HfO_2 (Fig 6a and 6b) indicate that all three samples have similar overall compositions. In Fig 6a, two international zircon standards are plotted for comparison. One is the internationally available zircon standard named 91500, analysed by Hoskin and Schaltegger (2003), although it should be noted that this standard zircon is from a large megacryst from

Ontario in Canada, with uncertain original lithology (Wiedenbeck et al., 1995). The second standard is zircon from the Mud Tank carbonatite (Hoskin and Ireland, 2000). Compared to other magmatic zircons, zircons associated with carbonatite typically have lower HREE/LREE ratios, less pronounced positive Ce anomalies and may lack a negative Eu anomaly (Rodionov et al., 2012).

Fig 6a demonstrates that both fenite zones display a typical igneous zircon chondrite-normalised REE profile, with a steep increase from LREE to HREE, a positive Ce anomaly and a negative Eu anomaly. The Eu anomaly may be attributable to redox conditions at time of formation or more likely because Eu^{2+} was preferentially partitioned into an alternative mineral, such as plagioclase. Compared to the standard zircons, Chilwa Island zircons are markedly chondrite-enriched across the whole REE spectrum. With reference to the Hf content of zircon (Fig 6b), performance of Student's t-Test did not reveal a conclusive difference between zircon from low- and medium-grade fenite. However, the PbO_2 plot of Fig 6c suggests a lower Pb content in the zircons from medium-grade fenite and the result of Student's t-Test indicated a significant difference in Pb content between zircon from the two different grades of fenite.

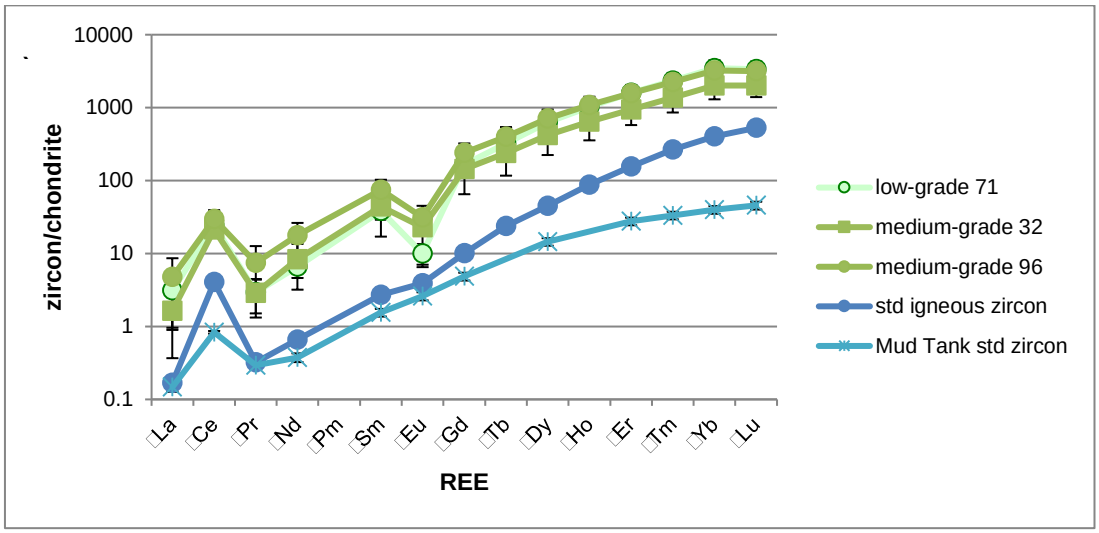

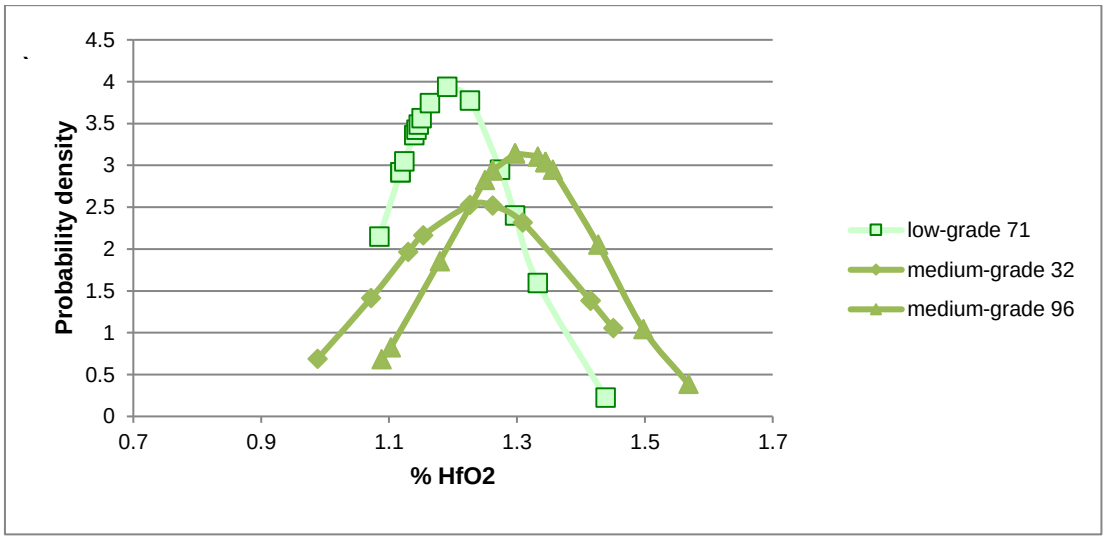

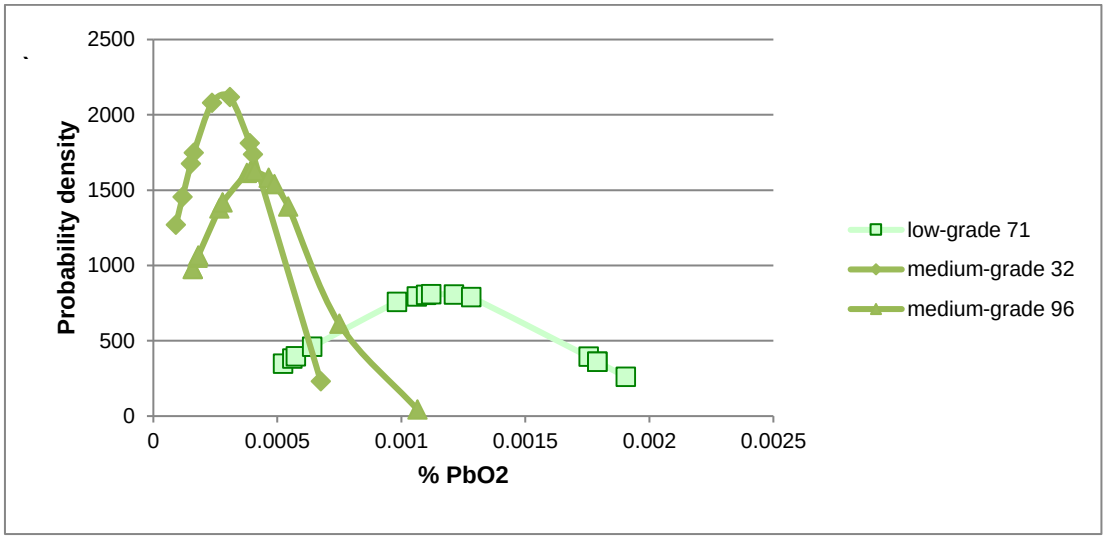

Fig 6 Minor and trace elements in zircon in Chilwa Island fenite

a) Chondrite-normalised (McDonough and Sun, 1995) REE abundances in Chilwa Island fenite zircon, with international standard zircon 91500 and zircon from the Mud Tank carbonatite plotted for comparison. Error bars represent one standard deviation. Chilwa Island zircon displays greater REE enrichment than either standard. Note also the presence of a negative Eu anomaly not seen in the standards

b) HfO_2 distribution curves for zircon with statistically insignificant difference in HfO_2 content between zircon in low-grade and medium-grade fenite

c) PbO_2 distribution curves for zircon showing zircon in medium-grade fenite with lower PbO_2 content than zircon in low-grade fenite

See supplementary data tables 5 and 6 for original data and see text for discussion of the significance of the graphs.

Th/U ratios are frequently used to distinguish magmatic from metamorphic zircon (Corfu et al., 2003, and references therein). The value of 0.2 is seen as key, with magmatic zircon commonly yielding ratios from 0.2 up to 1.0 or more. Zircon from carbonatite show particularly elevated values (Woolley and Kempe, 1989) with a remarkably high ratio of 9050 being found in a carbonatitic zircon from the ultramafic-alkaline-carbonatite complex of Kovdor in Russia by Rodionov et al. (2012). In contrast, metamorphic zircons in amphibolite-facies rocks typically have ratios of less than 0.2 (Corfu et al., 2003) and ratios are also low (<0.07) in metamorphic zircon in granulite rocks (Rubatto, 2002).

Th and U data, together with Th/U ratios for Chilwa Island zircons are presented in Supplementary Table 7. All values fall in the magmatic range, with zircon from low-grade fenite having a lower value of 0.37 on average than zircon in medium-grade fenite, which produced values between 0.56 and 0.71.

4.5 Classification of host rock from zircon composition - CART results

The zircon geochemical data, together with evidence gathered regarding zircon morphology and zoning, suggest that it might be appropriate to use the classification and regression trees (CART) that were developed by Belousova et al. (2002). These assign an origin by rock type to *magmatic* zircons in igneous rock, based on their composition. Although the samples in this study are found in metasomatised, metamorphic rock, Belousova et al. (2002) consider that inherited zircons of many felsic igneous or

metamorphic rocks carry potential information about the original source rock. Grains are run through the tree on a path detemined by binary switches defined by element concentration, or a ratio value, to end at a terminal node, which has been assigned a rock type label, and is the suggested parent rock. The shorter CART version is utilised here, as Belousova et al. (2002) designed this to use elements commonly reported in the literature and it is less reliant on the LREE, although it is recognised, that as in the longer version, it suffers from some ambiguity in assigning grantoid origin based on SiO_2 content.

The short CART results for the zircon analyses suggest that the parent rock type of zircon in both low-grade and medium-grade fenite was a granitoid containing up to 75% SiO_2 (Fig 7).

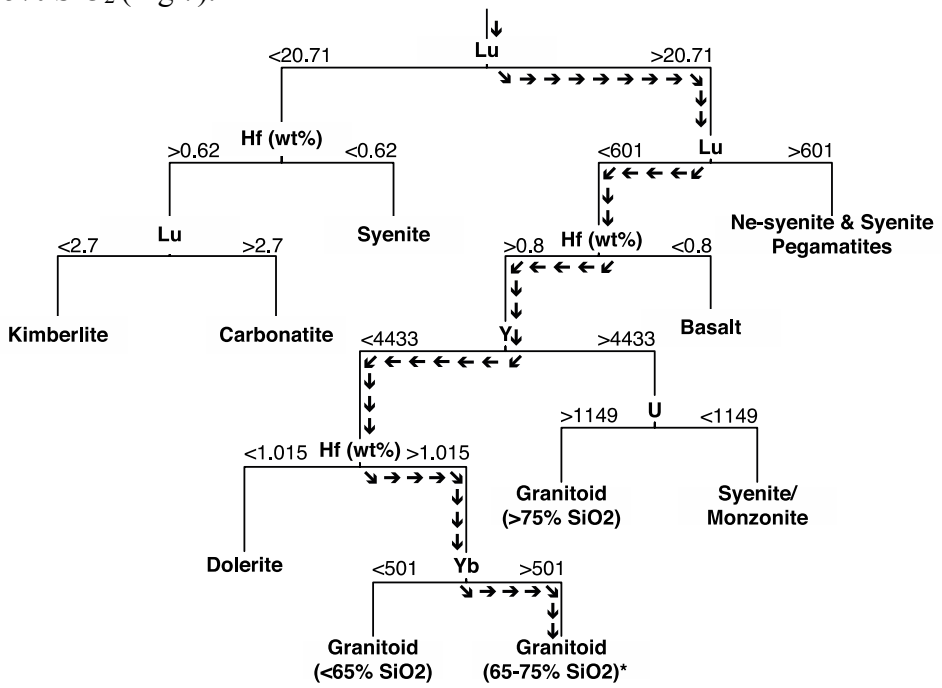

Fig 7 Short classification and regression (CART) tree results of zircon from both low- and medium-grade fenite indicating a granitoid origin for Chilwa Island zircon (* modified after Belousova et al., 2002)

4.6 Ti-in-zircon crystallisation temperatures

Titanium-in-zircon calculations were performed on zircons from both low-grade (BM1968 P37 71) and medium-grade fenite (BM1968 P37 32, BM1968 P37 96 and BM1968 P37 78) to establish crystallisation temperatures. Fenites at Chilwa Island contain both rutile and quartz, and the Ti-in-zircon thermometer equation from Watson et al. (2006), was applied therefore without using the modifications of Ferry and Watson (2007). Comparator data from more examples of zircon in low-grade fenite zircon would have been useful, but were not available and zircon in breccia is too resorbed to allow a precise analysis. Results are shown in Fig 8. Performance of Student's t-Test indicates a significant difference exists between the zircon samples from the two fenite zones. The crystallisation temperature of zircon from the lower grade fenite (temperature range 650-750˚C and mean of 698±11˚C) appears to be lower than for the zircons of the medium-grade fenite (temperature range of 700-1,000˚C, with means of 766±27˚C, 788±43˚C, 825±37˚C). The temperatures obtained are compatible with either a magmatic or a

metamorphic origin. Our interpretation that the older zircon from the low-grade fenite could represent an intrusive event, and the younger zircons found in the medium-grade fenite represent a later granulite facies event remains a possible explanation, if not conclusive. The results are strong evidence that both sets of zircon predate the fenitisation event because the crystallisation temperatures obtained are too high for this zircon to have a carbonatite or hydrothermal origin.

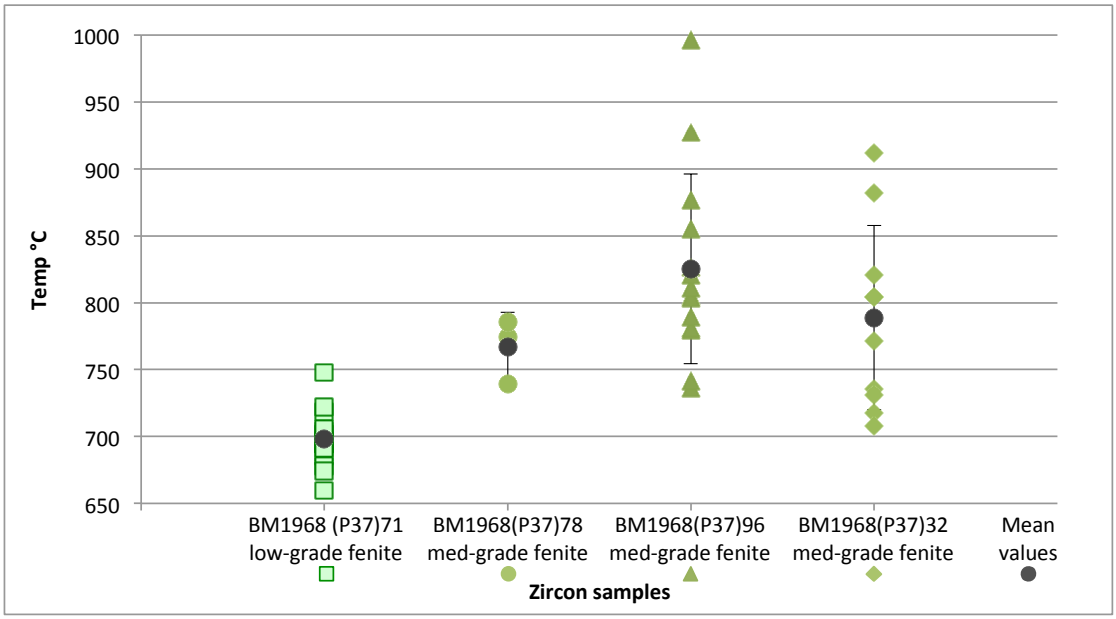

Fig 8 Ti-in-zircon crystallisation temperatures using Ti-in-zircon thermometer equation of Watson et al. (2006) showing difference in crystallisation temperature between zircon in low-grade fenite (BM1968 P37 71) and zircon in medium-grade fenite (BM1968 P37 78, BM1968 P37 96 and BM1968 P37 32) at Chilwa Island. Filled black circles indicate the mean temperature for each zircon sample and error bars represent one standard deviation.

4.7 Fluid inclusion data

Preliminary fluid inclusion studies were carried out on two samples of moderately fenitised quartz-bearing country rocks following the rationale, procedures and methods outlined by Bühn et al. (1999). The small size of the inclusions (<~10 µm) made observation difficult and ruled out detailed studies, especially in the inner fenite zones, where quartz is generally absent and inclusions in other minerals are too small or sparse for study.

Inclusion trails in the partly fractured and recrystallised quartz are complex and multi-compositional and may record both pre- and syn-fenitising fluid populations. Syn-fenitising fluid inclusions trails at Chilwa Island are recognised by their spatial coincidence within distinctive low-luminescent CL zones (Dowman, 2014), similar to that seen by Bühn et al. (2002) at the Okorusu fluorite deposit in Namibia.

The fluid inclusion assemblages occur within linear and curviplanar groupings. Variable proportions of liquid, vapour and solid phases are present in individual inclusions (Fig 9). Most notable are two- and three-phase CO_2(l)-CO_2(v)-aqueous inclusions and multiphase inclusions with several birefringent rounded and rhombic phases.

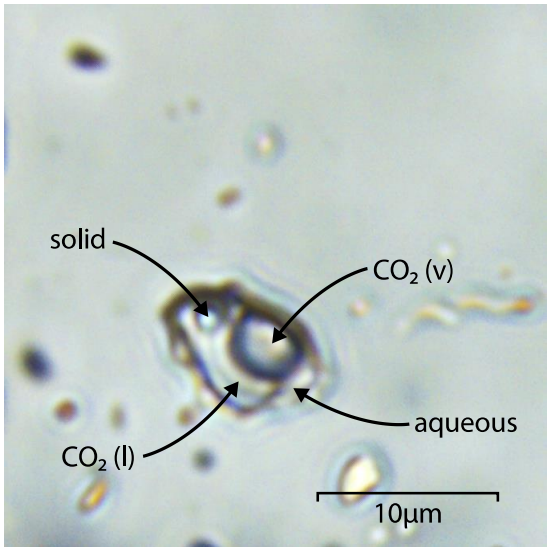

Fig 9 Multiphase fluid inclusion in quartz in Chilwa Island low-grade fenite BM1968 P37 130

Raman and microthermometric analysis of unopened inclusions and SEM-EDX analysis of the contents of opened inclusions were used to determine their compositions. CO_2(l+v) and H_2O(l) were the only fluid phases identified by Raman analysis. This was supported by limited microthermometric data (n=5) which showed melting of the CO_2 phase in frozen inclusions between -56.5˚C and -57.5˚C (±0.4˚C), which is close to the eutectic temperature of -56.6˚C for pure CO_2. Raman analysis of individual phases within multiphase inclusions showed typical Raman peaks (Supplementary Fig 1) for calcite (c.1081cm^{-1}), the REE-bearing carbonate burbankite (c.1076cm^{-1}), nahcolite, $NaHCO_3$ (c. 1044cm^{-1}) previously identified in fluid inclusions in fenite associated with carbonatite (Bühn and Rankin, 1999). An additional peak at 957cm^{-1} is ascribed to apatite. It was not possible to confirm these identities based on the limited compositional data available from SEM-EDX analyses of opened inclusions. However, several of the solid phases showed peaks for both Ca and Fe, suggesting the presence of calcitic and ankeritic carbonates. A Ti-Fe-bearing phase of flaky appearance was also tentatively identified as ilmenite. None of the solid phases showed detectable levels of Cl and it was not possible to determine if F and C are present due to the insensitivity of the method to light elements.

Microthermometric analysis was of limited value in determining the PVTX properties of the inclusions due to decrepitation above 250˚C. Some inclusions showed partial homogenisation and partial dissolution of solid phases below this temperature, but none achieved complete homogenisation before they decrepitated. The decrepitation was caused by the high internal pressures generated on heating inclusions with a moderate- to high-density CO_2 phase (c.0.5g/cm^3). The moderate to high densities and relative purity of the CO_2 contents were confirmed by measurements on five inclusions with CO_2 melting temperatures around -56˚C, and homogenisation of the CO_2 phase to CO_2 liquid at temperatures between -16˚C and -30.2˚C.

Unfortunately we were unable to determine low temperature eutectic temperatures (ice + salt hydrate + liquid) compatible with CO_2-Cl-HCO_3-bearing aqueous

fluids with any degree of certainty. This was due to difficulty in distinguishing phase changes involving clathrates, salt hydrate and ice.

In the context of whether the fluids contain significant chloride, it is noteworthy that neither halite nor any other chloride phase has been identified by SEM-EDX. Further evidence supporting this comment is that preliminary ICP-MS analysis of individual inclusions failed to detect any Cl above background (D. Banks, pers. comm.).

5. Discussion

5.1 Origin of Chilwa Island zircon

The ages of 769±5 Ma for the zircon from low-grade fenite, and of 529±2.3 Ma and 516±2.9 Ma for medium-grade fenite clearly exclude an origin for the zircon that has any direct relation to the Chilwa Island Carbonatite, which does not itself contain any zircon. This finding is supported by Ti-in-zircon temperatures, which are too high for hydrothermal zircon, or for zircon associated with *carbonatite* magma. Chilwa Island zircons do not possess the spongy textures and high HfO_2 content associated with hydrothermal zircon (Corfu et al., 2003; Hoskin, 2005; Wang et al., 2010). Zircon morphology in low- and medium-grade fenite is predominantly euhedral with well-defined terminations This size (mostly between 40 and 100 μm) and the shape of Chilwa Island zircons contrast with the large size of carbonatitic zircons, which are generally >250 μm in length (Campbell et al., 2014, and references therein), and the characteristic Fennoscandian carbonatitic zircon di-pyramidal form (Tichomirowa et al., 2013), or pyramid-dominant morphology of zircon associated with an origin from alkaline-carbonatite melt (Campbell et al., 2014). Furthermore, Chilwa Island zircon REE profiles do not fit with those of carbonatitic zircon, which are typically less steep and lack a Eu anomaly (Rodionov et al., 2012).

If a carbonatitic or metasomatic origin can be excluded, zircon could thus either have been part of the protolith or have formed during metamorphism associated with Pan African events. However, metamorphic zircon are generally characterised by subrounded and highly resorbed shapes, often with sector zoning or a structureless or patchy appearance (Corfu et al., 2003), and Th/U ratios of < 0.2. A metamorphic origin for Chilwa Island zircon therefore does not fit the evidence. Although grains containing cores are present at Chilwa Island, which is a texture often associated with metamorphic zircon, this is a feature common also in zircon in many igneous rocks and is thought to indicate crystallisation during multiple melt pulses (Chew et al., 2017; Corfu, 2013). Thus, the evidence of zircon shape and size, together with oscillatory growth zones in grains, Th/U ratios and anomalies for Ce and Eu, supports a (non-carbonatite) magmatic origin (Hoskin and Schaltegger, 2003). The CART results are consistent with a granitic origin.

5.2 Multiple zircon populations?

One explanation for more than one zircon age could be that the medium-grade fenite rocks host a different population of zircon from that found in low-grade fenite. However, this suggestion is not supported either by the mineral morphological examination or by the CART results.

Ti-in-zircon results suggest that zircon in low-grade fenite may have crystallised at lower temperatures than zircon in medium-grade fenite. However, the crystallisation temperatures calculated are compatible with either a magmatic or a metamorphic origin.

Geochemical analysis revealed no clear distinction between the zircon of the different fenite grades with respect to Hf and REE content. The keys to explaining the two ages lie in the Pb analyses, which show that the younger-dated zircons contain less Pb, and in the discordia line of the concordia plot (Fig 4d). Our interpretation is that zircons in medium-grade and low-grade fenite have the same origins, with those in the medium-grade rock undergoing a greater extent of resetting by subsequent metamorphic events, represented by the lower intercept on Fig 4d.

However, a secondary zircon population is considered to exist in the form of the sub-micron-sized zircon precipitated in porous apatite and rutile in medium-grade fenite. This is also observed at Kangankunde (Dowman, 2014).

5.3 The impact of Pan African events on zircon mineralogy

The earlier date of 770 Ma obtained from the Chilwa Island low-grade fenite zircons indicates that they are contemporaneous either with magma generated by intra-continental rifting during the break-up of the Rodinia supercontinent (Kröner, 2001; Kröner et al., 2001), or with the formation of Gondwana (~800 to ~550 Ma) (Kröner et al., 2001), an event which was accompanied by extensive granitoid magmatism of predominantly calc-alkaline chemistry over a period of ~840 to <600 Ma. Crystallisation temperatures obtained for zircon in low-grade fenite are compatible with formation in felsic to calc-alkaline magma (Helmy et al., 2004; Fu et al., 2008).

The later dates of ~520 Ma of the Chilwa Island medium-grade fenite zircons and the lower intercept of the line of discordia (Fig 4) may be associated with the high-grade metamorphism that took place in the Mozambique tectonic belt around 571-549 Ma (Kröner and Stern, 2005) following the aggregation of Gondwana.

Ages similar to the zircon dates reported here were recorded by Ashwal et al. (2007) who dated zircon and monazite from nepheline-bearing gneiss in the Mozambique Belt in southern Malawi. The euhedral shapes, oscillatory zoning and Th/U ratios of the zircon suggested a magmatic origin. Zircon dating yielded a mean age of 729±7 Ma, interpreted as being the time of magmatic crystallisation. Further dating of monazite, and discordance of some zircon data was indicative of a metamorphic event at 522±17 Ma during continental collision. This last event caused partial Pb-loss during local recrystallisation of zircon but did not destroy its magmatic characteristics.

These observations are in accord with experimental findings. Firstly, Sinha et al. (1992) showed that losses of Pb in non-metamict zircons from biotite granodiorite in Canada, and from gneiss in the USA could be induced at amphibolite-grade conditions but that the Hf content of the zircon was unaffected. Secondly, Harlov and Dunkley (2010) experimented with reacting non-metamict euhedral zircon and various alkali- and Ca-bearing fluids at 900˚C and 1,000 MPa. They found that in all experiments, radiogenic

^{206}Pb was strongly depleted in the altered zircon but that Hf concentrations remained unaltered. They concluded that the internal geochronometer of zircons can be reset due to the loss of radiogenic Pb. An amphibolite- to granulite-grade Pan African metamorphic event, as postulated by Ashwal et al. (2007), may therefore have been sufficient to cause this to occur, with some zircon crystals being totally reset, and other zircon grains being partially reset. Normal discordance seen in Chilwa Island zircons is indicative of Pb loss, and the plotting of a line of discordia (Fig 4) suggests a metamorphic reset at around 520 Ma.

It is therefore suggested that at Chilwa Island, magmatic zircon formed during the early Pan African events, and then underwent metamorphism later in the orogenic cycle. These metamorphic fluid pathways or lineaments may have persisted over time or have been reactivated (Woolley and Bailey, 2012; Brassinnes et al., 2005; Bailey, 1977), and could have been utilised by fluids expelled during the much later emplacement of carbonatite magma at ~135 Ma, thus leading to the association of carbonatite-derived minerals with the Pan African zircon. Although geochronological evidence does not indicate that any of the Chilwa primary zircon is contemporaneous with the carbonatite, there is tantalising evidence of precipitation in medium-grade fenite of secondary sub-micron zircon crystals, too small to date, in porous apatite and rutile, including the possible development of zircon grain rims associated with apatite.

5.4 Carbonatite-derived metasomatic fluids and element mobility

The response of zircon to the metasomatic fluids associated with carbonatite emplacement varies across the aureole. In the more intensely metasomatised zones, which are generally closest to the carbonatite, zircon grains are clearly dissolving or breaking down (Fig 3). Zr released in this process does not appear to be reprecipitated into Zr-bearing alkali-rich minerals. Zircon is not an abundant mineral in the inner aureole and Zr liberated by zircon breakdown may largely be disseminated throughout the much greater volume of rock comprising the outer aureole. Occasional examples of reprecipitated zircon of a few microns in size are found in apatite in the more altered medium-grade fenite.

In contrast to the dissolution observed in the inner aureole, in less altered medium-grade fenite, inherited zircon appears to be the nucleus for metasomatic minerals, and Zr may form overgrowths, too small to analyse, on zircon grains.

This contrast in zircon behaviour suggests that the zones in the aureole were dominated either spatially or temporally by fluids with different characteristics, and it is likely that a sequence of multiple fluids associated with carbonatite emplacement metasomatised the country rock at Chilwa Island (Dowman et al., 2017). We now consider the properties of the fluids in the inner aureole that dissolved zircon and any other pre-existing minerals (either relict or deposited by earlier fluids), but which inhibited further mineral precipitation. We then compare these fluids to those fluids that altered lower-grade fenite, where primary zircon has remained immobile and focused the formation of carbonatite-derived mineral assemblages and where a limited precipitation of secondary zircon has occurred,

5.5 The inner aureole: alkaline fluids, zircon dissolution and element mobilisation

Recognising that primary zircon is not always in equilibrium with its environment, Geisler et al. (2007) explored zircon-fluid reactions. Experiments indicated that alteration of zircon by fluid can occur either by dissolution coupled with overgrowth or by fluid-aided coupled dissolution-reprecipitation. In the latter process, zircon is replaced by a new, re-equilibrated zircon or by a new mineral phase. Harlov (2015) investigated the nature of fluids that could react with zircon. Combining non-metamict zircon with a series of alkali- and Ca-bearing fluids produced reactions that partially replaced zircon via coupled dissolution-reprecipitation, and produced some overgrowth of compositionally altered zircon (Harlov and Dunkley, 2010). Campbell et al. (2014) also refer to high Na activity in the fenitising fluids that altered rim zircon at Bayan Obo. In contrast, at Chilwa Island, no evidence of reprecipitation of the dissolved zircon is seen in the inner aureole, but Ayers et al. (2012) comment that where zircon is susceptible to dissolution and reprecipitation, this process can sometimes involve intervening transport.

The presence of alkaline fluids, possibly in combination with further ingredients to promote complexing with Zr and the REE, may be essential for element mobility, but Na is unlikely to be the primary alkali active in fluids responsible for zircon dissolution at Chilwa Island. It is not present in the few minerals found in the potassic inner aureole, which include pyrochlore of Ba- rather than Na-bearing composition. With regard to the effect of the proportion Na:K, experiments on zircon solubility by Watson (1979) suggested that Na_2O:K_2O ratios were much less important than the ratio (Na_2O + K_2O)/Al_2O_3, but it is clear that at Chilwa Island, zircon dissolution is favoured in the rocks of the inner aureole that contain a high proportion of K (Fig 3). Potassic fluids at Chilwa Island appear to have been limited spatially and zircon remained relatively unaffected in the more sodic outer regions.

Fluorine is commonly considered to be an important complexing agent but its role in fluids generally, and in alkaline fluids particularly, is contentious and not fully understood. Migdisov and Williams-Jones (2014) propose that in F-bearing systems, the REE are transported predominantly as non-fluoride complexes. They suggest chloride complexes as being especially stable, but Cl was not found in fluid inclusions at Chilwa Island, and halite was not positively identified. However, F has been claimed to increase zircon solubility and Zr mobility in magma-derived hydrothermal fluids in alkaline to peralkaline rocks (Salvi et al., 2000; Sheard et al., 2012), as well as the mobility of the HFSE generally in hydrous granitic melts (Keppler, 1993). High concentrations of Zr, Ti and REE were measured in highly alkaline (pH = 12), Na- and F-rich groundwaters from the Lovozero massif (Ayers et al., 2012 citing Kraynov et al., 1969). At Chilwa Island, rocks throughout the aureole, particularly in medium-grade fenite, contain fluorine in minerals such as fluorapatite, bastnäsite, parisite and pyrochlore (Dowman, 2014), and we therefore conclude that F was probably present in fenitising fluids at Chilwa Island. However, if F was also present in those fluids at Chilwa Island that did *not* dissolve zircon, fluorine alone cannot be the key ingredient in increasing zircon solubility.

Discounting the likelihood of Na and/or F acting alone in the inner aureole fluids at Chilwa Island, further fluid components may be important in mobilising Zr. Possible fluid components were suggested by Agangi et al. (2010) and references therein, who comment that high concentrations of F in melts promote incompatible behaviour of Zr

and the HFSE, which together with other complexing agents such as CO_2, OH and P, are then partitioned into fluids exsolved at the late magmatic stage. Campbell et al. (2014) also attribute the corrosion of zircon at Bayan Obo to an aggressive Na-rich, P- and F-bearing fluid. However, no trace of a fluid of this nature remains in the inner aureole at Chilwa Island, but it could have been active in the alteration of lower-grade fenite, as evidenced by the presence of sodic minerals and apatite beyond the inner regions.

Zircon is also known to be unstable in carbonate *magmas* (Barker, 2001; Wall et al., 2008). Although carbonate veins at Chilwa Island are few, there is evidence that zircon is not stable in such veins (Fig 10), and zircon is absent from carbonate-rich fenite at the Kangankunde carbonatite complex in Malawi (Dowman, 2014). However, the inner aureole of Chilwa Island contains little carbonate, and it is therefore unlikely to have been the main agent of zircon dissolution.

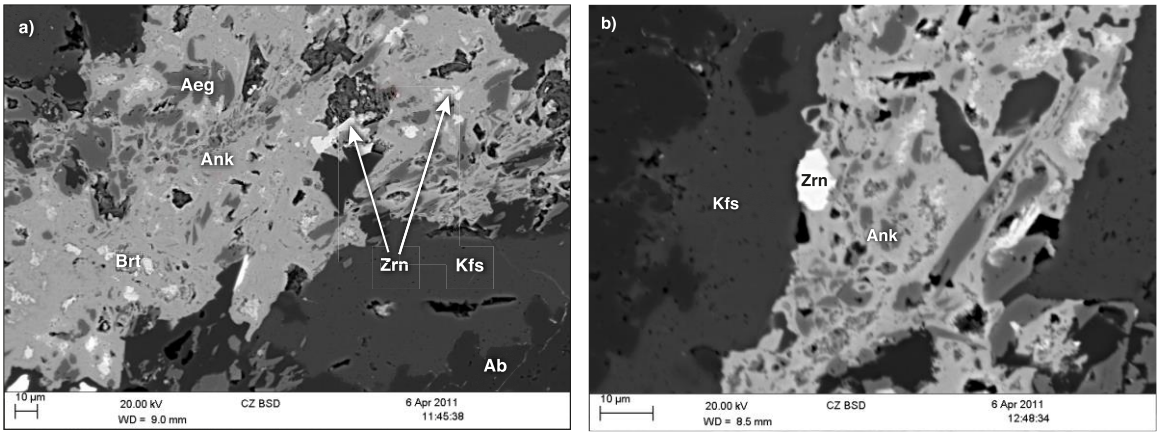

Fig 10 Zircon dissolving in ankerite vein in low-grade fenite BM1968 P37 130

Ayers et al. (2012) investigated zircon solubility in alkaline aqueous fluids and suggest that solubility is enhanced by highly alkaline, silica-rich fluids. The action of silica could be relevant at Chilwa Island if fluids reacted with country rock, and may explain the presence of certain areas of the aureole that are formed of secondary quartz, and devoid of zircon. Ayers et al. (2012) found that zircon solubility appeared to rise with increasing hydroxyl concentrations in fluids. It is not known whether this could be applicable at Chilwa Island. More altered parts of the aureole do not contain fluid inclusions suitable for investigation but the outer aureole hosts aqueous inclusions and water would have been a volatile in metasomatic fluids. However, the fluids favoured by us as causing the dissolution of zircon in the inner aureole would be similar to those described by Rubie and Gunter (1983). In their work on alkaline fluids and fenitisation, these authors examined potassium metasomatism and brecciation around carbonatites (similar to that at Chilwa Island), and surmised that this could involve fluids very rich in CO_2 and/or temperatures up to 600˚C. At Chilwa Island, fluids of this nature could have created a potassic inner aureole, stripping away any pre-existing mineralogy, at a relatively late stage (Dowman et al., 2017). The fluids were evidently restricted in extent, not reaching the outer aureole. Thus a high temperature (500-600˚C), potassic, CO_3^{2-} or CO_2-rich fluid, probably containing F, and possibly involving some SiO_2 and/or hydroxyl activity, is invoked as dissolving zircon and mobilising Zr and HFSE.

5.6 The outer aureole: agents of mineral precipitation

HFSE- and REE-bearing minerals were precipitated from metasomatic fluids in medium-grade fenite. These fluids did not dissolve zircon. In contrast, zircon appears to have focused the formation of carbonatite-derived mineral micro-assemblages comprising REE-bearing apatite (dated by fission track as contemporary with the carbonatite) plus Nb-bearing ilmenite, Nb-bearing rutile, barite and the rare earth minerals, monazite, bastnäsite and parisite. Further supporting evidence of the carbonatitic origin of these fluids is provided by the investigation of the fluid inclusions from this zone and the low-grade fenite zone, which demonstrated that inclusions contained CO_2, together with elements associated with carbonatites, such as REE, Sr, Ba, as well as carbonate, in daughter minerals such as nahcolite and burbankite. The compositions, distributions and heterogeneity of the inclusions at Chilwa Island are similar to the fluid inclusion assemblages reported by Bühn and Rankin (1999) for post-magmatic, carbonatite-derived, carbothermal fluids in the country rocks surrounding some Namibian carbonatites.

Fluid components that promote the deposition of HFSE and the REE include F, which Migdisov and Williams-Jones (2014) consider to be the principal agent promoting REE precipitation. Precipitation may be induced by processes that increase fluid pH or decrease its temperature, or by the introduction of a new ligand into the system. Campbell et al. (2014) write of high concentrations of the REE, already mobilised by F^- or by CO_3^{2-} that could form complexes with phosphate in hydrothermal or metasomatic fluids, leading to the precipitation of the RE-bearing minerals bastnäsite, monazite, parisite and some apatite. These minerals are all present in medium-grade fenite at Chilwa Island, and could have been deposited from similar fluids. Ayers et al. (2012) cite Hoskin and Schaltegger (2003) and Schaltegger (2007) in referring to the formation of hydrothermal zircon, possibly analogous to the secondary zircon at Chilwa Island, in low- to medium-temperature hydrothermal deposits associated with F-rich or alkaline fluids.

Mineral precipitation caused by an increase in fluid pH is not considered likely in the fluids that were expelled from carbonatite and passed into carbonate-poor country rock at Chilwa Island. Deposition may have been triggered by the introduction or interaction of ligands and/or decreasing temperature as fluids moved outwards through the aureole. Multiple episodes of fluid events are most likely to have occurred. Alkaline alteration by fluids of a sodi-potassic nature was probably a separate event to that of mineralisation from fluorine-, CO_3^2.-, and P-bearing fluids. Precipitation occurred of REE, Ba and Nb mobilised from the carbonatites, and to a limited extent, of Zr mobilised from the inner aureole. The fluid properties are summarised in Table 1.

Table 1 Summary of the properties of dominant fluids in the inner and outer parts of the aureole

Property of dominant fluid and its effect on rocks	**Proximal to carbonatite - 'dissolving' zircon**	**Distal to carbonatite – 'nucleus' zircon**
Effect on minerals	Removal of pre-existing minerals, zircon dissolution, no evidence of reprecipitated Zr	Zircon appears stable and nucleates carbonatite-derived minerals. Limited precipitation of secondary grains
Alkali component		

	K, little Na, breccias almost monophase K-feldspar	Na (and plagioclase) increasingly dominant over K (and orthoclase) with distance from carbonatite
F content (from whole-rock analysis, Dowman, 2014)	Highest just outside breccias where fluorapatite and fluorcarbonates present	Present but diminishes with distance, following decrease in F-bearing minerals
Temperature	Up to 600˚C in breccia? (Rubie and Gunter, 1983)	Lower, due to distance from carbonatite but fluid inclusion studies indicate temperature to be at least 200˚C in outer fenite zones (Dowman, 2014)
CO_2:H_2O content	Loss on ignition (volatile) values are low in breccia and highest in fenite where some carbonate present (Dowman, 2014). CO_2 maybe dominant in inner fenite zones (Rubie and Gunter, 1983)	Ratio not known, but CO_2 may diminish with distance and lower fluid temperatures, with H_2O increasingly dominant (Smith et al., 2000)
Salinity	Not known, possibly higher due to lower H_2O	Presence of nahcolite but no confirmed halite suggest c. 20% wt. eq. NaCl

6. Conclusions and implications

The contrasts in behaviour of zircon are evidence of spatial and temporal variations in metasomatising fluids across the fenite aureole. Multiple fluid episodes are thus considered to have contributed to fenitisation at Chilwa Island.

Zircon is a key component of the mineral assemblages in fenite at Chilwa Island. However, the use of zircon geochronology alone to date the mineral assemblages present in the fenites at Chilwa Island would have been misleading. At 520 and 770 Ma old the zircon separates collected from the fenite aureole are significantly older than the 136 Ma old carbonatite, and originate from Pan African events and not from fenitisation. It is known that relicts of earlier assemblages may be preserved during metasomatism or metamorphism (Harlov and Austrheim, 2013; Zharikov et al., 2007; Yardley and Bodnar, 2014). However, in this study, the initial assumption, based on petrographic observations, was that all phases present in the intricate apatite-ilmenite-zircon micro-mineral assemblages were contemporaneous. This has been proved incorrect. A simple acceptance of the zircon ages as dating the metasomatic event would have implied that the event was not related to emplacement of the carbonatite intrusion. This suggests that care is required when using zircon crystals to date metasomatic assemblages. Similar geological environments where these conditions might occur are those in general where fluids promote mineralisation and, in particular, in alkaline environments where Zr is hosted mostly within zircon, rather than being mobilised into secondary, less refractory minerals, such as gittinsite (Strange Lake) or steenstrupine (Ilimaussaq).

Although the zircon age data reported in this study do not reflect that of the fenite micro-mineral assemblages, the presence of older zircon, even as a primary phase within these assemblages, is important because it appears to have encouraged the initial nucleation in the fenite of other, non-structurally related minerals, such as apatite. Although the fenitising fluids may have followed reactivated pathways exploited previously by fluids associated with the East African orogeny, this would only partially explain the spatial overlap of the zircon and fenite assemblages. The relationship seems to be more important than this, as metasomatic apatite growing in the fenite precipitated in very close association with the zircon on which it nucleated (Fig 2c-f). The affinity of

apatite with zircon becomes stronger as the degree of alteration increases until, in the medium-high grade fenite, embayments and partial inclusions of apatite suggest incipient zircon dissolution during nucleation. Pyrochlore similarly nucleated on and replaced zircon that was undergoing dissolution in the most intensely metasomatised 'high-grade' fenite in the innermost part of the aureole. The reasons for these associations require further investigation. However, as far as we are aware, this behaviour of zircon acting as a nucleus for metasomatic assemblages of other minerals has not been previously reported.

Acknowledgements

Thanks are due to Anatole Beams for help in the paper layout, and to Richard Giddens at Kingston University for his assistance with the SEM instrument.

*This paper is dedicated to the memory of Teresa Jeffries who passed away on 18th April 2016. Teresa was instrumental in setting up this project and was responsible for collecting the LA-ICP-MS zircon chemistry and age data reported here.

Bibliography

Agangi, A., Kamenetsky, V., McPhie, J., 2010. The role of fluorine in the concentration and transport of lithophile trace elements in felsic magmas: Insights from the Gawler Range Volcanics, South Australia. Chemical Geology 273, 314-325.

Ashwal, L., Armstrong, R., Roberts, R., Schmitz, M., Corfu, F., Hetherington, C., Burke, K., Gerber, M., 2007. Geochronology of zircon megacrysts form nepheline-bearing gneisses as constraints on tectonic setting: implication for resetting of the U-Pb and Lu-Hf isotopic systems. Contrib. to Mineral. Petrol. 153 SRC-, 389–403.

Ayers, J.; Zhang, L.; Luo, Y.; Peters, T., 2012. Zircon solubility in alkaline aqueous fluids at upper crustal conditions. Geochimica et Cosmochimica Acta 96, 18-28.

Bailey, D., 1977. Lithospheric control of continental rift magmatism. Geol. Soc. London J. 133 SRC-, 103–106.

Barker, D., 2001. Calculated silica activities in carbonatite liquids. Contrib. to Mineral. Petrol. 141 SRC-, 704–709.

Belousova, E., Griffin, W., O'Reilly, S., Fisher, N., 2002. Igneous zircon: trace element composition as an indicator of source rock type. Contrib. to Mineral. Petrol. 143 SRC-, 602–622.

Berger, V., Singer, D., Orris, G., Brassinnes, S., Balaganskaya, E., Demaiffe, D., 2009. Carbonatites of the world, explored deposits of Nb and REE; database and grade and tonnage models. US Geol. Surv. Open-File Rep. 2009-1139 85 SRC-, 76–92.

Brassinnes, S., Balaganskaya, E., Demaiffe, D., 2005. Magmatic evolution of the differentiated ultramafic, alkaline and carbonatite intrusion of Vuoriyarvi (Kola Peninsula, Russia). A LA-ICP-MS study of apatite. Lithos 85, 76–92. doi:10.1016/j.lithos.2005.03.017

Bühn, B., Rankin, A., Schneider, J., Dulski, P., 2002. The nature of orthomagmatic, carbonatitic fluids precipitating from REE, Sr-rich fluorite: fluid inclusion evidence from the Okorusu fluorite deposit, Namibia. Chemical Geology 186, 75-98.

Bühn, B., Rankin, A., Radtke, M., Haller, M., Knöchel, A., 1999. Burbankite, a (Sr,REE,Na,Ca)-carbonate in fluid inclusions from carbonatite-derived fluids: Identification and characterisation using Laser Raman spectroscopy, SEM-EDX and synchrotron micro-XRF analysis. American Mineralogist 84, 1117-1125.

Bühn, B., Rankin, A., 1999. Composition of natural, volatile-rich Na-Ca-REE-Sr carbonatitic fluids trapped in fluid inclusions. Geochim. Cosmochim. Acta 63, 3781–3797.

Campbell, L., Compston, W., Sircombe, K., Wilkinson, C., 2014. Zircon from the East Orebody of the Bayan Obo Fe-Nb-REE deposit, China, and SHRIMP ages for carbonatite-related magmatism and REE mineralization events. Contributions to Mineralogy and Petrology 168: 1041.

Chew, D., Petrus, J., Kenny, G., McEvoy, N., 2017 Rapid high-resolution U-Pb LA-Q-ICPMS age mapping of zircon. J.Anal. At. Spectrometry. 32, 262-276.

Corfu, F., 2013. A century of U-Pb geochronology: The long quest towards concordance. GSA Bulletin. 125 (1/2), 33-47.

Corfu, F., Hanchar, J., Hoskin, P., Kinny, P., 2003. Atlas of Zircon Textures. Reviews in Mineralogy and Geochemistry 53, 469-500.

Coulson, I., Chambers, A., 1996. Patterns of zonation in Rare-earth-bearing minerals in nepheline syenites of the North Qôroq Centre, South Greenland. The Canadian Mineralogist 34, 1163-1178.

Dowman, E., Wall, F., Treloar, P., Rankin, A., 2017. Rare earth mobility as a result of multiple phases of fluid activity in fenite around the Chilwa Island Carbonatite, Malawi. In Press Mineralogical Magazine DOI: https://doi.org/10.1180/minmag.2017.081.007.

Dowman, E., 2014. Mineralisation and fluid processes in the alteration zone around the Chilwa Island and Kangankunde carbonatite complexes, Malawi. Kingston University, UK.

Eby, G., Roden-Tice, M., Krueger, H., Ewing, W., Faxon, E., Woolley, A., 1995. Geochronology and cooling history of the northern part of the Chilwa Alkaline Province, Malawi. J. African Earth Sci. 20, 275–288.

Ferry, J., Watson, E., 2007. New thermodynamic models and revised calibrations for the Ti-in-zircon and Zr-in-rutile thermometers. Contrib. to Mineral. Petrol. 154 SRC-, 429–437.

Fu, B., Page, F., Cavosie, A., Fournelle, J., Kita, N., Lackey, J.S., Wilde, S., Valley, J., 2008. Ti-in-zircon thermometry: applications and limitations. Contrib. to Mineral. Petrol. 156 SRC-, 197–215.

Galbraith, R., 1982. Statistical analysis of some fission-track counts and neutron fluence measurements. Nuclear Tracks 6, 99-107.

Garson, M., 1965. Carbonatites in Southern Malawi. The Government Printer, Zomba, Malawi.

Garson, M., Campbell Smith, W., 1958. Chilwa Island. The Government Printer, Zomba, Malawi.

Geisler, T., Schaltegger, U., Tomaschek, F., 2007. Re-equilibration of Zircon in Aqueous Fluids and Melts. Elements 3, 43-50.

Goodenough, K., Wall, F., Merriman, D., 2017. The Rare Earth Elements: Demand, Global Resources, and Challenges for Resourcing Future Generations. Natural Resources Research. DOI:10.1007/s11053-017-9336-5.

Götze, J., Kempe, U., Habermann, D., Nasdala, L., Neuser, R., Richter, D., 1999. High-Resolution Cathodoluminescence Combined with SHRIMP Ion Probe Measurements of Detrital Zircons. Mineralogical Magazine 63(2), 179-187.

Hanchar, J., Finch, R., Hoskin, P., Watson, E., Cherniak, D., Mariano, A., 2001. Rare earth elements in synthetic zircon: Part 1. Synthesis, and rare earth element and phosphorus doping. American Mineralogist 86, 667-680.

Harley, S., Kelly, N., 2007. Zircon Tiny but Timely. Elements 3 SRC-G, 13–18.

Harlov, D., Austrheim, H., 2013. Metasomatism and the Chemical Transformation of Rock. Springer-Verlag, Berlin Heidelberg.

Harlov, D., Dunkley, D., 2010. Experimental high-grade alteration of zircon using alkali-and Ca-bearing solutions: resetting the zircon geochronometer during metasomatism. V41D-2301 presented at Fall. Meeting, AGU, San Francisco, 13-17 Dec 2010.

Harlov, D., 2015. Fluids and Geochronometers: Charting and Dating Mass Transfer During Metasomatism and Metamorphism. Journal of the Indian Institute of Science 95:2, 109-123.

Hayward, C., Jones, A., 1991. Cathodoluminescence petrography of Middle Proterozoic extrusive carbonatite from Qasiarsuk, South Greenland. Mineralogical Magazine 55, 591-603.

Heinrich, E., 1966. The Geology of Carbonatites. Rand McNally, Chicago.

Helmy, H., Ahmed, A., El Mahallawi, M., Ali, S., 2004. Pressure, temperature and oxygen fugacity conditions of calc-alkaline granitoids, Eastern Desert of Egypt, and tectonic implications. J. African Earth Sci. 38 SRC-, 255–268.

Hogarth, D., 1989. Pyrochlore, apatite and amphibole: distinctive minerals in carbonatite. In: Bell, K. (Ed.), Carbonatites: Genesis and Evolution. Unwin Hyman, pp. 105-148.

Hoskin, P., Ireland, T., 2000. Rare earth element chemistry of zircon and its use as a provenance indicator. Geology 28 SRC-, 627–630.

Hoskin, P., Schaltegger, U., 2003. The composition of Zircon and Igneous and Metamorphic Petrogenesis. Rev. Mineral. Geochemistry 53 SRC-, 27–62.

Hoskin, P., 2005. Trace-Element Composition of Hydrothermal Zircon and the Alteration of Hadean Zircon from the Jack Hills, Australia. Geochim. Cosmochim. Acta. 69 (3) 637-648.

Hurford, A., 1990. Standardization of fission track calibration: recommendation by the Fission Track Working Group of the IUGS Subcommission on Geochronology. Chem. Geol. 80 SRC-, 171–178.

Kempe, U., Götze, J., 2002. Cathodoluminescence (CL) behaviour and crystal chemistry of apatite from rare-metal deposits. Mineral. Mag. 66, 151–172.

Keppler, H., 1993. Influence of fluorine on the enrichment of high field strength trace elements in granitic rocks. Contrib. to Mineral. Petrol. 114 SRC-, 479–488.

Ketcham, R., 2005. Forward and inverse modelling of low-temperature thermochronometry data. Rev. Mineral. Geochem 58 (1), 275-314.

Ketcham, R., Carter, A., Donelick, R., Barbarand, J., Hurford, A., 2007. Improved modelling of fission-track annealing in apatite. American Mineralogist 92, 789-798.

Kraynov, S., Mer'kov, A., Petrova, N., Baturinskaya, L., Zharikova, V., 1969. Highly alkaline (pH 12) fluorsilicates in the deeper zones of the Lovozero massif. Geochem. Int. 6, 635-640.

Kröner, A., Collins, A., Hegner, E., Muhongo, S., Willner, A., Kehelpannala, K., 2001. Has the East African Orogen Played Any Role in the Formation and Breakup of the Supercontinent Rodinia and the Amalgamation of Gondwana? New Evidence from Field Relationship and Isotopic Data. Gondwana Res. 669–671.

Kröner, A., Stern, R., 2005. Pan-African Orogeny. Encycl. Geol. 1 SRC-Go, 1–12.

Kröner, A., Wan, Y., Liu, X., Liu, D., 2014. Dating of zircon from high-grade rocks: Which is the most reliable method? 2014. Geoscience Frontiers. 5 (4) 439-620.

Kröner, A., Willner, A.P., Hegner, E., Jaeckel, P., Nemchin, A., 2001. Single zircon ages, PT evolution and Nd isotopic systematics of high-grade gneisses in southern Malawi and their bearing on the evolution of the Mozambique belt in southeastern Africa. Precambrian Res. 109, 257–291. doi:10.1016/S0301-9268(01)00150-4

Kröner, A., 2001. The Mozambique belt of East Africa and Madagascar: significance of zircon and Nd model ages for Rodinia and Gondwana supercontinent formation and dispersal. South African J. Geol. 104, 151–166.

Le Bas, M., 2008. Fenites associated with carbonatites. Can. Mineral. 46 SRC-, 915–932.

Le Bas, M., 1981. Carbonatite magmas. Mineral. Mag. 44 SRC-, 133–140.

Mariano, A., 1989. Nature of economic mineralisation in carbonatites and related rocks., in: Bell, K. (Ed.), Carbonatites: Genesis and Evolution. Unwin Hyman, pp. 147-176.

Mariano, A., 1988. Some further geological applications of cathodoluminescence. In Marshall, D. , Mariano, A. Cathodoluminescence of Geological Material. Unwin Hyman, Boston. pp. 94-123.

McDonough, W., Sun, S., 1995. The composition of the Earth. Chem. Geol. 120 SRC-, 223–253.

Migdisov, A., Williams-Jones, A., 2014. Hydrothermal transport and deposition of the rare earth elements by fluorine-bearing aqueous liquids. Miner. Deposita. 49, 987-997.

Mitchell, R., 2015. Primary and secondary niobium mineral deposits associated with carbonatites. Ore Geology Reviews 64, 626-641.

Rae, D., Coulson, I., Chambers, A., 1996. Metasomatism in the North Qôroq Centre, South Greenland: apatite chemistry and rare-earth element transport. Mineralogical Magazine 60, 207-220.

Rodionov, N., Belyatsky, B., Antonov, A., Kapitonov, I., Sergeev, S., 2012. Comparative in-situ U-Th-Pb geochronology and trace element composition of baddeleyite and low-U zircon from carbonatites of the Palaeozoic Kovdor alkaline-ultramafic complex, Kola Peninsula, Russia. Gondwana Research 21, 728-744.

Rubatto, D., 2002. Zircon trace geochemistry: partitioning with garnet and the link between U-Pb ages and metamorphism. Chemical Geology 184, 123-138.

Rubie, D., Gunter, W., 1983. The Role of Speciation in Alkaline Igneous Fluids during Fenite Metasomatism. Contrib. to Mineral. Petrol. 82 SRC-, 165–175.

Rubin, J., Henry, C., Price, J., 1993. The mobility of zirconium and other "immobile" elements during hydrothermal alteration. Chem. Geol. 110 SRC-, 29–47.

Salvi, S., Fontan, F., Monchoux, P., Williams-Jones, A., Moine, B., 2000. Hydrothermal Mobilisation of High Field Strength Elements in Alkaline Igneous Systems: Evidence from the Tamazeght Complex (Morocco). Econ. Geol. 95 SRC-, 559–576.

Schaltegger, U., 2007. Hydrothermal zircon. Elements 3, 51.

Sheard, E., Williams-Jones, A., Heiligmann, M., Pederson, C., Trueman, D., 2012. Controls on the concentration of Zirconium, Niobium, and the Rare Earth Elements in the Thor Lake Rare Metal Deposit, Northwest Territories, Canada. Econ. Geol. 107 SRC-, 81–104.

Siebel, W., Shang, C., Theru, E., Danišik, M., Rohrmüller, J., 2012. Zircon response to high-grade metamorphism as revealed by U-Pb and cathodoluminescence studies. Int. J. Earth Sci. 101, 2105–2123.

Sinha, A., Wayne, D., Hewitt, D., 1992. The hydrothermal stability of zircon: Preliminary experimental and isotopic studies. Geochim. Cosmochim. Acta 56 SRC-, 3551–3560.

Smith, M., Henderson, P., Campbell, L., 2000. Fractionation of the REE during hydrothermal processes: Constraints from the Bayan Obo Fe-REE-Nb deposit, Inner Mongolia, China. Geochim. Cosmochim. Acta 64, 3141–3160.

Snelling, N., 1965. Age determinations on three African carbonatites. Nature 205 SRC-, 491.

Tichomirowa, M., Whitehouse, M., Gerdes, A., Götze, J., Schulz, B., Belyatsky, B., 2013. Different zircon recrystallisation types in carbonatites caused by magma mixing: Evidence from U-Pb dating, trace element and isotope composition (Hf and O) of zircons from two Precambrian carbonatites from Fennoscandia. Chem. Geol. 353 SRC-, 173–198.

Tsuchiya, Y., Kayama, M., Nishido, H., Noumi, Y., 2015. Annealing effects on cathodoluminescence of zircon. Journal of Mineralogical and Petrological Sciences 110, 283-292.

Verplanck, P., Mariano, A.N., Mariano, A., 2016. Rare earth element ore geology of carbonatites. In Verplanck, P., Hitzman, M., (Eds.) Rare earth and critical elements in ore deposits. Vol. Reviews in Economic Geology 18. Society of Economic Geologist, Littleton, Colorado. pp. 5-32.

Verplanck, P., Van Gosen, B., 2011. Carbonatite and Alkaline Intrusion-Related Rare Earth Element Deposits-A Deposit Model. https://pubs.usgs.gov/of/2011/1256/report/OF11-1256.pdf%0A

Wall, F., Niku-Paavola, V.S., Müller, A., Jeffries, T., 2008. Xenotime-(Y) from carbonatite dykes at Lofdal, Namibia: unusually low LREE:HREE ratio in carbonatite, and the first dating of xenotime overgrowths on zircon. Can. Mineral. 46 SRC-, 861–877.

Wang, R., Griffin, W., Chen, J., 2010. Hf content and Zr/Hf ratios in granite zircons. Geochemical Journal 44, 65-72.

Watson, E., Wark, D., Thomas, J., 2006. Crystallisation thermometers for zircon and rutile. Contrib. to Mineral. Petrol. 151 SRC-, 413–433.

Watson, E., 1979. Zircon saturation in felsic liquids: Experimental results and applications to trace element geochemistry. Contr. Mineral. and Petrol. 70, 407-419. DOI:10.1007/BF00371047.

Waychunas G., 2002. Luminescence of Natural and Synthetic Apatites. Reviews in Mineralogy and Geochemistry 48 (1), 701-742.

Wiedenbeck, M., Allé, P., Corfu, F., Griffin, W., Meier, M., Oberli, F., 1995. Three zircon standards for U-Th-Pb, Lu-Hf, trace element and REE analyses. Geostand. Newsl. 19 SRC-, 1–23.

Woolley, A., 1969. Some aspects of fenitisation with particular reference to Chilwa Island and Kangankunde, Malawi. Bull. Br. Museum Nat. Hist. 2, 191-219.

Woolley, A., 2001. Alkaline Rocks and Carbonatites of the World Part 3: Africa. The Geological Society, London.

Woolley, A., Bailey, D., 2012. The crucial role of lithospheric structure in the generation and release of carbonatites: geological evidence. Mineral. Mag. 76, 259–270.

Woolley, A., Kempe, D., 1989. Carbonatites: nomenclature, average chemical compositions, and element distribution. In Bell, K. (Ed.) Carbonatites: Genesis and Evolution, Unwin Hyman, London. pp 1-14.

Yardley, B., Bodnar, R., 2014. Fluids in the continental crust. Geochemical Perspectives 3, 1-123.

Zharikov, V., Pertsev, N., Rusinov, V., Callegari, E., Fettes, D., 2007. Metasomatism and metasomatic rocks. Recommendations by the IUGS Subcommission on the Systematics of Metamorphic Rocks: Web Version 01.02.07. https://www.bgs.ac.uk/scmr/docs/papers/paper_9.pdf

Supplementary data

Supplementary Table 1 Chilwa Island fenite samples. Last three samples used only for mineralogical investigation, and do not have whole-rock analyses

NHM number	NHM rock type classification	Fenite grade used in this study
BM1968 P37 63	Quartz fenite	Medium
BM1968 P37 71	Quartz fenite	Low
BM1968 P37 72	Quartz fenite	Low
BM1968 P37 78	Quartz fenite	Medium
BM1968 P37 96	Quartz fenite	Medium
BM1968 P37 101	Quartz fenite	Medium
BM1968 P37 130	Quartz fenite	Low
BM1968 P37 32	Syenite fenite	Medium
BM1968 P37 54	Syenite fenite	Medium/high
BM1968 P37 68	Syenite fenite	Medium/high
BM1968 P37 102	Syenite fenite	Medium/high
BM1968 P37 139	Breccia	Breccia
BM1968 P37 146	Breccia	Breccia
BM1968 P37 100	Quartz fenite	Medium
BM1968 P37 126	Quartz fenite	Medium
BM1968 P37 137	Syenite fenite	Medium/high

Supplementary Table 2 LA-ICP-MS U-Pb isotope data for zircon in fenite at Chilwa Island

a) BM1968 P37 71 low-grade fenite

	Isotopic ratios and errors						**Ages and errors**			
	207Pb/ 235U	±2σ %	206Pb/ 238U	±2σ %	207Pb/ 206Pb	±2σ %	207Pb/ 235U	±2σ % Ma	206Pb/ 238U	±2σ % Ma
concordant data										
fe19b08	0.8283	2.94	0.0979	1.44	0.0611	2.76	613	13	602	8
fe19b05	0.8420	2.66	0.1001	2.30	0.0601	2.60	620	12	615	13
fe19a15	0.9164	3.06	0.1060	1.86	0.0627	2.44	660	15	650	12
fe19b14	0.9433	3.86	0.1086	1.22	0.0625	2.22	675	19	664	8
fe19a09	1.0031	3.46	0.1159	1.52	0.0637	2.76	705	18	707	10
fe19a13	1.0769	3.04	0.1206	1.68	0.0648	1.62	742	16	734	12
fe19b12	1.1196	2.02	0.1249	1.68	0.0646	1.78	763	11	758	12
fe19b06	1.1504	2.96	0.1262	1.52	0.0657	2.16	777	16	766	11
fe19a07	1.1398	1.66	0.1269	1.32	0.0652	1.46	772	9	770	10
fe19b16	1.1512	1.96	0.1272	1.54	0.0655	1.16	778	11	772	11
discordant data										
fe19a16	0.8810	4.82	0.0944	2.78	0.0663	3.10	641	23	581	15
fe19b07	0.8792	4.16	0.0953	2.88	0.0662	2.50	641	20	587	16
fe19b11	0.8743	2.90	0.1004	1.50	0.0615	2.26	638	14	617	9
fe19a08	0.9533	2.04	0.1059	1.46	0.0661	2.16	680	10	649	9
fe19a10	0.9440	1.78	0.1083	1.34	0.0626	1.52	675	9	663	8
fe19b09	1.6314	2.76	0.1095	2.22	0.1081	3.80	982	17	670	14
fe19b13	0.9706	2.56	0.1097	2.04	0.0637	2.16	689	13	671	13
fe19a12	0.9770	1.46	0.1099	1.76	0.0637	1.46	692	7	672	11
fe19a06	0.9833	1.94	0.1112	1.82	0.0635	1.64	695	10	680	12
fe19610	1.0137	1.50	0.1135	1.42	0.0633	1.92	711	8	693	9
fe19a14	1.0886	1.98	0.1198	1.76	0.0646	1.58	748	11	730	12
fe19a11	1.1200	1.98	0.1241	1.26	0.0653	1.20	763	11	754	9
fe19a05	1.2020	3.08	0.1300	1.32	0.0663	1.92	802	17	788	10
fe19b15	1.1543	2.68	0.1300	1.50	0.0647	1.62	779	15	788	11

b) BM1968 P37 32 medium-grade fenite

	Isotopic ratios and errors						Ages and errors			
	207Pb/ 235U	±2σ %	206Pb/ 238U	±2σ %	207Pb/ 206Pb	±2σ %	207Pb/ 235U	±2σ % Ma	206Pb/ 238U	±2σ % Ma
concordant data										
mr29b11	0.6537	3.00	0.0822	1.92	0.0584	2.86	511	12	509	9
mr29b14	0.6571	3.42	0.0821	2.58	0.0573	3.12	513	14	509	13
mr29a06	0.6623	4.12	0.0824	2.16	0.0578	3.56	516	17	510	11
mr29b09	0.6626	4.10	0.0823	2.14	0.0589	3.22	516	17	510	11
mr29a07	0.6639	5.42	0.0828	2.62	0.0587	6.88	517	22	513	13
mr29a05	0.6633	2.54	0.0833	2.46	0.0576	2.44	517	10	516	12
mr29b10	0.6567	6.46	0.0833	2.28	0.0592	5.46	513	26	516	11
mr29a15	0.6719	2.82	0.0838	2.02	0.0578	2.34	522	11	519	10
mr29a11	0.6699	1.84	0.0843	1.38	0.0583	2.04	521	7	522	7
mr29a10	0.6708	3.02	0.0848	2.34	0.0576	3.32	521	12	525	12
discordant data										
mr29a13	0.6019	7.86	0.0789	2.86	0.0546	7.00	478	30	489	13
mr29b16	0.6650	11.38	0.0795	2.70	0.0614	8.12	518	46	493	13
mr29b08	0.6665	7.84	0.0831	5.06	0.0574	6.60	519	32	515	25
mr29a14	0.6990	3.52	0.0843	2.22	0.0606	4.16	538	15	522	11
mr29b13	0.6232	8.80	0.0844	2.80	0.0554	6.92	492	34	522	14
mr29b12	0.7204	4.72	0.0852	1.62	0.0608	4.86	551	20	527	8
mr29a12	0.7567	4.70	0.0861	2.46	0.0616	3.36	572	21	533	13
mr29a16	0.7564	3.68	0.0863	2.46	0.0622	5.02	572	16	534	13
mr29a09	0.7096	7.14	0.0866	2.44	0.0579	5.98	545	30	536	13
mr29b07	0.6893	6.16	0.0874	2.46	0.0586	5.30	532	26	540	13
mr29b15	0.6932	4.96	0.0875	2.48	0.0567	4.34	535	21	541	13
mr29a08	0.6510	6.16	0.0893	3.40	0.0530	7.14	509	25	551	18
mr29b05	0.7003	5.54	0.0894	2.24	0.0584	5.04	539	23	552	12
mr29b06	0.6651	6.70	0.0913	2.52	0.0536	7.46	518	27	563	14

c) BM1968 P37 96 medium-grade fenite

	Isotopic ratios and errors						Ages and errors			
	207Pb/ 235U	±2σ %	206Pb/ 238U	±2σ %	207Pb/ 206Pb	±2σ %	207Pb/ 235U	±2σ % Ma	206Pb/ 238U	±2σ % Ma
concordant data										
mr31a16	0.6624	4.18	0.0831	2.80	0.0587	4.14	516	17	515	14
mr31a10	0.6757	8.08	0.0836	4.56	0.0594	9.10	524	33	518	23
mr31b09	0.6714	6.90	0.0838	5.00	0.0582	4.62	522	28	519	25
mr31b11	0.6686	3.04	0.0839	2.50	0.0578	3.44	520	12	519	13
mr31a13	0.6681	3.18	0.0839	2.70	0.0588	3.94	520	13	520	14
mr31a15	0.6676	4.14	0.0845	3.04	0.0574	3.90	519	17	523	15
mr31b05	0.6701	5.44	0.0852	2.54	0.0578	5.70	521	22	527	13
mr31b06	0.6884	5.74	0.0853	3.34	0.0582	6.76	532	24	527	17
mr31a08	0.6960	4.72	0.0874	2.46	0.0578	3.56	536	20	540	13
mr31a12	0.7333	3.74	0.0903	3.52	0.0583	3.62	559	16	557	19
discordant data										
mr31b08	0.7083	4.68	0.0819	3.70	0.0609	3.76	544	20	508	18
mr31b13	0.6909	5.22	0.0823	3.16	0.0590	3.90	533	22	510	15
mr31b10	0.6852	1.82	0.0830	2.30	0.0588	2.44	530	8	514	11
mr31b12	0.6903	5.26	0.0835	2.80	0.0592	4.92	533	22	517	14
mr31b14	0.6457	3.12	0.0842	4.18	0.0590	3.96	506	12	521	21
mr31b15	0.6818	4.50	0.0841	2.00	0.0591	5.72	528	19	521	10
mr31a09	0.6714	2.72	0.0853	2.08	0.0580	3.30	522	11	528	11
mr31a14	0.7107	5.20	0.0855	2.38	0.0597	4.32	545	22	529	12
mr31b16	0.7016	3.44	0.0860	3.02	0.0585	3.10	540	14	532	15
mr31a11	0.7008	3.10	0.0861	1.18	0.0597	2.66	539	13	533	6

mr31a05	0.6934	3.64	0.0901	3.18	0.0574	3.46	535	15	556	17
mr31a07	0.7068	6.60	0.0901	3.12	0.0578	7.64	543	28	556	17
mr31b07	0.7458	4.16	0.0941	1.92	0.0577	3.92	566	18	580	11
mr31a07	0.6979	4.68	0.0943	2.62	0.0560	4.88	538	20	581	15

Supplementary Table 3 - Fission track analytical data for BM1968 P37 71

No of crystals	Dosimeter		Spontaneous		Induced		Age Dispersion		Central Age (Ma) ±1s	Mean track length (μm)	S.d.	No of tracks
	ρd	Nd	ρs	Ns	pi	Ni	$P\chi^2$	$RE_{\%}$				
20	1.422	5911	2.143	1114	5.216	2691	40.4	3.8	98.7±3.8	12.90±0.16	1.62	101

(i) track densities are (x106 tr cm^{-2}) numbers of tracks counted (N) shown in brackets

(ii) analyses by external detector method using 0.5 for the 4□/2□ geometry correction factor

(iii) ages calculated using dosimeter glass CN-5; (apatite) □CN5 =339±5
calibrated by multiple analyses of IUGS apatite and zircon age standards (see Hurford 1990)

(iv) P□2 is probability for obtaining □2 value for v degrees of freedom, where v = no. crystals - 1

(v) central age is a modal age, weighted for different precisions of individual crystals (see Galbraith 1992)

Supplementary Table 4 SEM-EDS analyses of apatite in fenite and carbonatite at Chilwa Island

Low-grade fenite												n=3
	SiO_2	CaO	SrO	Na_2O	P_2O_5	La_2O_3	Ce_2O_3	Pr_2O_3	Nd_2O_3	F	O = F	Total
Representative	0.77	52.87	1.47	0.61	38.87	0.48	1.19	n.d.	0.64	3.58	1.51	98.97
Std deviation	0.40	0.90	0.24	0.42	0.21	0.11	0.12		0.10	0.47		
Medium-grade fenite grain rims												n=12
	SiO_2	CaO	SrO	Na_2O	P_2O_5	La_2O_3	Ce_2O_3	Pr_2O_3	Nd_2O_3	F	O = F	Total
Representative	1.62	51.89	1.19	0.06	39.72	0.49	1.23	0.23	0.75	3.49	1.47	99.20
Std deviation	0.39	0.62	0.23	0.02	0.11	0.01	0.16	0.01	0.17	0.19		
Medium-grade fenite grain cores												n=12
	SiO_2	CaO	SrO	Na_2O	P_2O_5	La_2O_3	Ce_2O_3	Pr_2O_3	Nd_2O_3	F	O = F	Total
Representative	0.83	53.29	0.67	0.07	41.39	0.16	0.42	0.05	0.29	3.75	1.57	99.35
Std deviation	0.27	0.30	0.27	0.03	0.28	0.04	0.12	0.02	0.11	0.18		
Medium/high-grade fenite RE-rich grains												n=15
	SiO_2	CaO	SrO	Na_2O	P_2O_5	La_2O_3	Ce_2O_3	Pr_2O_3	Nd_2O_3	F	O = F	Total
Representative	1.04	50.17	2.53	0.75	39.73	1.10	2.00	0.16	0.57	3.42	1.44	100.03
Std deviation	0.31	0.22	0.92	0.11	0.64	0.37	0.39	0.08	0.12	0.43		
Medium/high-grade fenite RE-poor grains												n=4
	SiO_2	CaO	SrO	Na_2O	P_2O_5	La_2O_3	Ce_2O_3	Pr_2O_3	Nd_2O_3	F	O = F	Total
Representative	n.d.	52.90	2.79	0.53	40.78	0.48	1.15	0.15	0.45	2.42	1.02	100.63
Std deviation		2.13	0.81	0.24	0.77	0.09	0.04	0.09	0.15	0.79		
Carbonatite												n=7
	SiO_2	CaO	SrO	Na_2O	P_2O_5	La_2O_3	Ce_2O_3	Pr_2O_3	Nd_2O_3	F	O = F	Total
Representative	0.63	52.18	2.73	0.22	40.97	0.13	0.36	n.d.	0.10	3.13	1.32	99.13
Std deviation	0.11	0.86	0.39	0.13	0.42	0.09	0.14	n.d.	0.07	0.67		

Note: Y not analysed n.d. = not detected

Supplementary Table 5 Laser ablation analysis of REE, Hf and Pb in ppm in zircon in fenite at Chilwa Island

a) BM 1968 P37 71 low-grade fenite

	La	Ce	Pr	Nd	Sm	Eu	Gd	Tb	Dy	Ho	Er	Tm	Yb	Lu	Hf	Pb
oc25a03	0.23	12.90	0.22	3.26	8.04	0.30	43.10	14.60	195.00	66.80	300.00	70.40	657.00	87.80	9530	9.53
oc25a04	0.14	17.80	0.21	3.88	8.41	0.93	50.10	17.00	225.00	80.60	365.00	81.20	786.00	115.00	9200	15.50
oc25a05	<0.02	15.10	0.11	2.19	5.38	0.61	31.10	11.20	147.00	54.10	249.00	56.10	533.00	83.20	9720	10.50
oc25a06	1.83	21.30	0.57	5.26	10.60	1.01	56.50	21.70	283.00	106.00	487.00	116.00	1210.00	156.00	9480	22.30
oc25a07	2.44	20.80	0.96	6.96	5.66	0.55	29.90	10.20	139.00	49.80	229.00	53.80	514.00	79.40	9660	9.70
oc25a08	0.03	18.40	0.11	2.71	5.66	0.57	38.50	14.00	187.00	68.10	309.00	67.50	604.00	102.00	10100	15.20
oc25a09	<0.02	17.60	0.13	2.83	5.90	0.55	36.00	12.50	170.00	60.50	275.00	62.50	619.00	89.50	9870	16.50
oc25a10	0.21	18.50	0.16	2.64	5.88	0.65	35.00	12.20	162.00	59.50	273.00	61.30	575.00	87.30	9480	11.10
oc25a11	0.89	8.85	0.33	1.89	1.86	0.18	9.98	3.91	53.90	21.60	106.00	26.30	273.00	42.70	12200	4.53
oc25a12	<0.01	8.19	0.05	0.88	2.76	0.13	19.10	6.47	78.70	25.80	106.00	21.90	189.00	31.40	11000	5.55
oc25a13	<0.01	8.54	0.03	0.80	2.38	0.15	15.50	5.62	77.60	28.70	136.00	31.70	312.00	50.20	10800	4.98
oc25a14	0.01	10.90	0.12	2.72	6.77	0.65	41.70	14.40	196.00	72.30	336.00	74.60	688.00	114.00	10400	9.20
oc25a15	0.08	7.00	0.11	1.14	2.89	0.17	15.70	5.38	62.40	19.70	79.30	16.60	146.00	25.70	11300	4.85
oc25a16	0.73	16.00	0.46	4.25	5.99	1.43	33.20	10.90	144.00	50.80	223.00	52.00	507.00	71.20	9760	8.51
oc25a17	1.55	21.40	0.53	3.81	6.99	0.58	41.60	15.20	205.00	75.90	340.00	78.80	777.00	111.00	9690	15.50
Average	0.74	14.89	0.27	3.01	5.68	0.56	33.13	11.69	155.04	56.01	254.22	58.05	559.33	83.09	10146	10.90
Std dev	0.84	5.10	0.26	1.67	2.42	0.36	13.31	4.86	65.14	24.33	112.29	26.26	268.68	35.19	836.09	5.18

b) BM 1968 P37 32 medium-grade fenite

	La	Ce	Pr	Nd	Sm	Eu	Gd	Tb	Dy	Ho	Er	Tm	Yb	Lu	Hf	Pb
mr29c03	0.65	13.60	0.19	2.10	3.13	0.59	16.00	4.99	63.70	22.20	99.90	22.40	221.00	34.70	10700	0.79
mr29c04	0.01	8.95	0.03	0.47	1.11	0.13	7.31	2.84	38.70	15.40	78.20	19.90	200.00	36.10	12300	3.37
mr29c05	0.20	15.30	0.62	10.20	15.70	4.00	60.60	17.10	186.00	59.30	238.00	49.60	437.00	69.10	9580	1.41
mr29c06	<0.02	16.10	0.19	3.28	6.36	1.68	28.00	8.45	98.20	32.10	138.00	30.40	295.00	43.10	9780	1.02
mr29c07	<0.01	9.14	0.02	0.47	1.09	0.12	6.87	2.54	34.90	13.60	67.00	16.30	163.00	27.90	12000	1.31
mr29c09	0.13	10.30	0.22	2.40	4.56	0.93	23.80	7.14	85.20	30.50	130.00	28.90	278.00	43.50	10400	2.67
mr29c10	1.07	11.60	0.22	1.53	1.44	0.26	7.67	2.86	41.40	16.30	81.00	20.40	213.00	36.00	11100	3.48
mr29c11	0.55	15.00	0.45	6.37	12.20	1.44	59.60	18.40	216.00	72.90	298.00	65.40	584.00	86.00	9090	5.85
mr29c12	0.10	17.60	0.48	7.60	12.90	2.47	48.50	13.50	165.00	53.60	228.00	51.40	508.00	68.70	8380	2.05
Average	0.39	13.07	0.27	3.82	6.50	1.29	28.71	8.65	103.23	35.10	150.90	33.86	322.11	49.46	10370	2.44
Std dev	0.38	3.18	0.21	3.44	5.67	1.28	22.15	6.23	68.88	21.67	83.35	17.33	150.57	20.03	1303.61	1.61

c) BM 1968 P37 96 medium-grade fenite

	La	**Ce**	**Pr**	**Nd**	**Sm**	**Eu**	**Gd**	**Tb**	**Dy**	**Ho**	**Er**	**Tm**	**Yb**	**Lu**	**Hf**	**Pb**
mr31c04	<0.03	17.60	0.03	1.06	2.39	0.24	15.00	5.24	74.70	27.60	131.00	30.00	315.00	48.10	13300	2.30
mr31c06	<0.02	8.31	0.07	1.36	3.00	0.39	15.30	5.17	67.00	24.60	114.00	25.70	235.00	41.90	12100	1.57
mr31c07	0.05	12.50	0.46	7.83	12.80	1.68	58.20	18.50	211.00	68.80	297.00	63.80	580.00	87.80	11000	3.54
mr31c08	0.01	14.50	0.18	4.04	8.06	1.18	42.20	12.90	165.00	55.30	247.00	53.70	479.00	79.90	11400	3.27
mr31c09	8.11	33.10	2.85	21.30	15.40	2.48	56.30	16.50	198.00	64.20	276.00	62.40	597.00	84.00	9350	4.23
mr31c10	0.07	16.60	0.11	2.03	4.17	0.47	17.90	6.46	83.10	29.90	131.00	31.50	324.00	47.30	11000	2.41
mr31c11	0.09	17.70	0.65	10.90	16.00	2.50	71.00	20.30	242.00	81.50	342.00	76.10	677.00	99.30	10700	4.71
mr31c12	<0.03	17.50	0.40	6.00	11.70	1.50	51.30	15.30	186.00	64.40	274.00	60.50	586.00	83.90	11500	4.03
mr31c13	0.06	8.20	0.13	2.81	5.59	0.73	28.10	8.47	107.00	35.90	155.00	33.80	301.00	51.50	10700	1.54
mr31c14	0.08	20.50	0.72	13.10	23.80	2.91	114.00	33.30	399.00	127.00	510.00	105.00	924.00	140.00	10000	6.49
mr31c15	<0.02	13.20	0.05	1.04	2.73	0.30	12.40	4.43	58.90	23.90	113.00	28.30	304.00	45.20	11400	1.38
mr31c16	0.69	24.60	1.12	11.80	14.60	2.67	53.80	16.00	186.00	62.60	257.00	58.40	545.00	76.80	10600	3.38
mr31c17	0.10	8.17	0.56	10.60	13.30	3.09	58.40	16.70	180.00	61.30	249.00	49.60	422.00	74.50	9230	1.38
mr31c18	2.03	42.50	2.34	19.30	21.70	4.63	74.10	23.50	290.00	98.80	431.00	100.00	1000.00	127.00	11400	9.22
Average	0.81	18.21	0.69	8.08	11.09	1.77	47.71	14.48	174.84	58.99	251.93	55.63	520.64	77.66	10977	3.53
Std dev	2.17	9.73	0.87	6.70	6.99	1.32	28.62	8.20	95.42	29.97	119.91	25.37	232.10	30.13	1053.13	2.20

Supplementary Table 6 SEM-WDS analyses of zircon in fenite at Chilwa Island

Low-grade BM1968 P37 71						n=14
	SiO_2	ZrO_2	$Fe_2O_3(t)$	HfO_2	Total	
Representative	31.79	65.76	0.12	1.55	99.22	
Std deviation	0.65	0.43	0.08	0.18		
Medium-grade BM1968 P37 32						n=13
	SiO_2	ZrO_2	$Fe_2O_3(t)$	HfO_2	Total	
Representative	33.86	65.06	0.43	1.30	100.65	
Std deviation	0.43	0.72	0.03	0.27		
Medium-grade BM1968 P37 78						n=43
	SiO_2	ZrO_2	$Fe_2O_3(t)$	HfO_2	Total	
Representative	32.58	66.13	0.33	1.42	100.46	
Std deviation	0.27	0.30	0.27	0.03		
Medium-grade BM1968 P37 96						n=20
	SiO_2	ZrO_2	$Fe_2O_3(t)$	HfO_2	Total	
Representative	32.52	65.74	0.45	1.35	100.06	
Std deviation	1.10	1.31	0.09	0.31		
Breccia BM1968 P37 146						n=3
	SiO_2	ZrO_2	$Fe_2O_3(t)$	HfO_2	Total	
Representative	33.93	66.34	n.d.	0.48	100.75	
Std deviation	0.48	0.67		0.03		

n.d. = not detected

Supplementary Table 7 LA-ICP-MS analyses of Th and U in zircon in fenite at Chilwa Island

a) BM1968 P37 71

Sample no	Th ppm	U ppm	Th/U
oc25a03 03	142.00	378.00	0.38
oc25a04 04	234.00	460.00	0.51
oc25a05 05	158.00	372.00	0.42
oc25a06 06	324.00	970.00	0.33
oc25a07 07	149.00	437.00	0.34
oc25a08 08	239.00	470.00	0.51
oc25a09 09	246.00	618.00	0.40
oc25a10 10	179.00	405.00	0.44
oc25a11 11	65.10	295.00	0.22
oc25a12 12	101.00	215.00	0.47
oc25a13 13	82.40	412.00	0.20
oc25a14 14	138.00	334.00	0.41
oc25a15 15	98.80	474.00	0.21
oc25a16 16	133.00	387.00	0.34
oc25a17 17	262.00	642.00	0.41
Average	170.09	457.93	0.37
Std dev	75.20	178.73	0.10

b) BM1968 P37 32

Sample no	Th ppm	U ppm	Th/U
mr29c03 03	19.00	33.70	0.56
mr29c04 04	81.40	259.00	0.31
mr29c05 05	36.20	31.60	1.15
mr29c06 06	24.70	29.70	0.83
mr29c07 07	32.80	77.70	0.42
mr29c09 09	62.20	116.00	0.54
mr29c10 10	88.10	189.00	0.47
mr29c11 11	145.00	157.00	0.92
mr29c12 12	50.50	68.80	0.73
Average	59.99	106.94	0.56
Std dev	40.00	80.44	0.27

c) BM1968 P37 78

Sample no	Th ppm	U ppm	Th/U
oc28a04 04	171.00	206.00	0.83
oc28a05 05	56.80	78.10	0.73
oc28a06 06	76.70	151.00	0.51
Average	101.50	145.03	0.70
Std dev	61.01	64.16	0.16

d) BM1968 P37 96

Sample no	Th ppm	U ppm	Th/U
mr31c04 04	65.50	138.00	0.47
mr31c06 06	38.30	65.50	0.58
mr31c07 07	99.40	114.00	0.87
mr31c08 08	85.80	101.00	0.85
mr31c09 09	95.50	109.00	0.88
mr31c10 10	62.30	104.00	0.60
mr31c11 11	113.00	124.00	0.91
mr31c12 12	98.80	133.00	0.74
mr31c13 13	37.70	55.60	0.68
mr31c14 14	173.00	186.00	0.93
mr31c15 15	37.20	86.10	0.43
mr31c16 16	77.80	79.90	0.97
mr31c17 17	36.90	38.10	0.97
mr31c18 18	266.00	484.00	0.55
Average	91.94	129.87	0.71
Std dev	62.69	108.61	0.19

a)

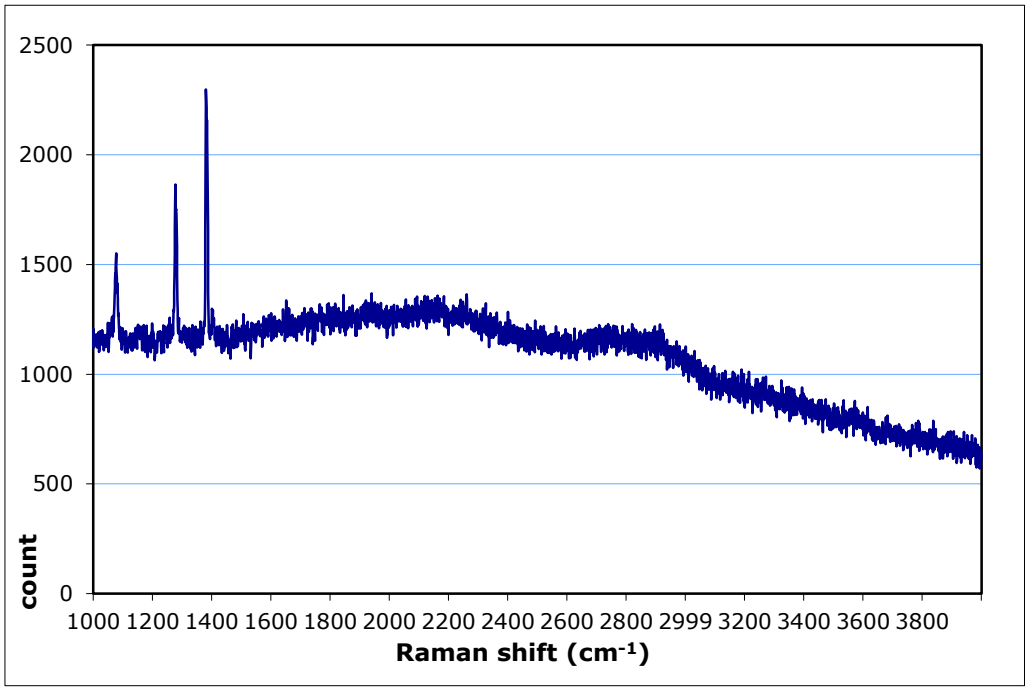

b)

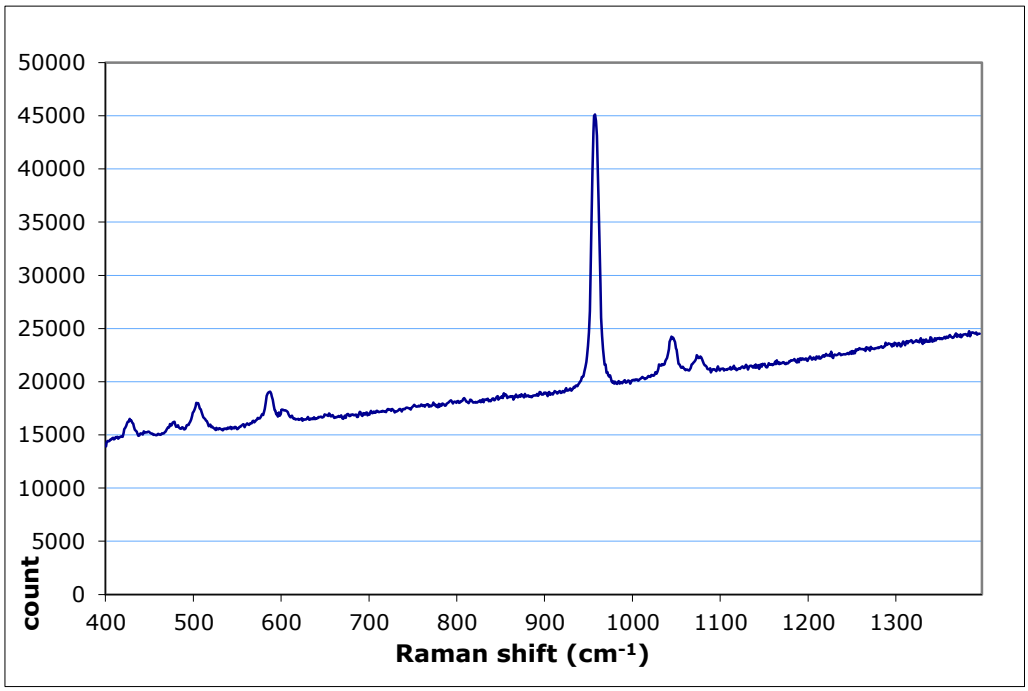

Supplementary Fig 1 Raman spectroscopic analysis of fluid inclusions in quartz in fenite at Chilwa Island

a) Low-grade fenite BM1968 P37 71 - fluid inclusion containing burbankite and calcite (peak 1 at 1074 to 1081) and CO_2 gas (peak 2 at 1278 & peak 3 at 1380) WIRE 1418

b) Medium-grade fenite BM1968 P37 78 – fluid inclusion containing apatite at 957 (peak 1), and nahcolite at 1044 (peak 2) and carbonate, possibly burbankite at 1073-1078 (peak 3) WIRE 1544